EFFECTS OF SURFACE ROUGHNESS ON HYDRODYNAMIC AND THERMAL BOUNDARY LAYERS

A Thesis Submitted

In Partial Fulfilment of the Requirements
for the Degree of

MASTER OF TECHNOLOGY

by

ARKALGUD RAMASWAMIAH SUBRAMANYA

to the

Department of Mechanical Engineering
INDIAN INSTITUTE OF TECHNOLOGY, KANPUR

September 1969

This work has been
dedicated to my dear parents

— Author

CERTIFICATE

Certified that the work ' Effects of Surface Roughness on Hydrodynamic and Thermal Boundary Layers ' has been carried out under my supervision and it has not been submitted elsewhere for a degree.

S. V. Patankar

S.V.Patankar
Assistant Professor
Department of Mechanical Engineering
Indian Institute of Technology, Kanpur

ABSTRACT

A finite-difference procedure for solving turbulent boundary layer equations developed by Patankar and Spalding has been applied to the case of the boundary-layer flow over a flat plate with surface roughness. Both hydrodynamic and thermal boundary layers have been considered. The roughness characteristics for various types of roughness have been correlated from pipe-flow results and predictions have been made for two types. Experiments on a plane wall jet on a rough surface were conducted and the agreement between the theory and the experiment was found to be satisfactory.

ACKNOWLEDGEMENTS

I am very much indebted to Dr. S.V.Patankar for suggesting me this interesting problem and express my deep sense of gratitude and sincere regards for him for providing continued guidance at all stages of the work. I am highly grateful to him for his constant encouragement, understanding and keen interest in the progress of the work.

I am thankful to the Mechanical Engineering Department for providing me the necessary equipment for carrying out the experiments. Finally, I am thankful to the staff of the Computer Centre, Indian Institute of Technology, Kanpur, for their co-operation.

A. R. Subramanya

CONTENTS

NOMENCLATURE

Symbol	Meaning
c_f	drag coefficient
E	term used in Couette-flow velocity profile expression
E_M	value of E for flow past a hydrodynamically smooth surface
h	the specific enthalpy
h^+	dimensionless enthalpy
$\tilde{h}$	the stagnation enthalpy
J	heat flux in positive y direction
k	a mixing-length constant
ℓ	the mixing length
p	pressure
p_r	spacing of two-dimensional roughness elements
P	resistance of the laminar sub layer
P_M	value of P of a smooth surface
r	distance from the axis of symmetry
R	a Reynolds number for the region near the wall
R_r	roughness Reynolds number
R_x	Reynolds number based on the distance along the distance *plate*
s	dimensionless shear stress at the wall

	dimensionless heat flux
	the Stanton number
	absolute temperature
	velocity in the longitudinal direction
	velocity of air injection at the slot
	dimensionless velocity the Couette-flow analysis
	distance in the stream-wise direction
	distance in the cross-stream direction
c	height of slot opening
i	a characteristic thickness of the layer
r	nominal height of roughness elements
r^+	dimensionless distance from the surface in the Couette-flow analysis
r_r^+	$\frac{y_r\sqrt{\tau_s/\rho}}{\nu}$
δ	boundary-layer thickness
β	coefficient in $E \sim y_r^+$ relationships for fully rough flow
λ	a mixing-length constant
μ	laminar viscosity of the fluid
μ_{eff}	effective viscosity of the fluid
ν	kinematic viscosity of the fluid
ρ	density of the fluid
σ	laminar Prandtl number
σ_{eff}	effective Prandtl number
σ_t	turbulent Prandtl number
τ	local shear stress
ψ	a stream function

ω	dimensionless stream function

Subscripts

K	the internal boundary of the layer
I	the external boundary of the layer
max	appertaining to the point where the velocity profile has a maximum
s	the condition at the wall
∞	the condition at the free stream
$\frac{1}{2}$	appertaining to the point where the velocity is half its maximum value

CHAPTER - 1

INTRODUCTION

1.1 The problem considered.

A study of the effects of surface roughness on the boundary-layer flow over a flat plate is reported in this thesis. Both hydrodynamic and thermal boundary layers are considered. The flow is assumed to be steady and two-dimensional. The plate is considered to be impermeable and the fluid incompressible.

The effect of roughness on the development of turbulent boundary layers is not only a subject of fundamental importance in fluid mechanics, but is also of importance in practical fields such as naval architecture, aeronautics and nuclear engineering. The broad field can be placed between two extremes: the desire to avoid roughness as shown by the ship builders and the attempt to introduce it deliberately to improve the heat transfer as practised by nuclear-reactor designers and others.

The roughness problem has become very important in aeronautical applications since the advent of laminar aerofoils, as the process of transition from laminar to turbulent flow depends on the roughness of the wall. In most practical applications connected with the flat plate, namely, ships, lifting surfaces of an aircraft, turbine blades etc., the surface cannot be considered hydrodynamically smooth. The smoothness of normally-manufactured surfaces is not sufficient to secure hydrodynamically smooth conditions. Consequently, the flow must

a rough plate is of great practical interest. However, unlike the smooth-wall-flow investigations, the number of different conditions under which the rough-wall flow have been examined to date is limited.

In the calculation of the drag on ships, it is important to consider the plates with very small roughness (painted metal plates) as well as smooth plates covered with single protuberances, such as rivet heads, welded seams, joints etc. A number of measurements on such surfaces in an open channel have been carried out.

It has been demonstrated that the laws of friction in flows along rough walls which have emerged from experimental investigations can be applied to the motion of natural winds over the surface of the earth. The effective roughness of surfaces covered with different kinds of vegetation could be determined by the measurements of the velocity distribution of the wind in the layer just above the surface of the earth.

The amount of roughness which is considered admissible in engineering applications is the maximum height of individual roughness elements which cause no increase in drag, compared with a smooth wall. The practical importance of determining the amount of admissible roughness for a given set of circumstances is very great, because it determines the amount of labour which it is worth spending in manufacturing a given surface.

1.2 Outline of the thesis

The present work aims at a study of the effects of surface roughness on the turbulent boundary-layer flow. However,

the theory of turbulence has not been fully developed because of its extremely complicated nature. Attempts have been made to investigate the turbulent motion with the help of semi-empirical hypotheses, which have been developed into more or less complete theories. However, none of them have succeeded in fully analysing the flow, and it has become necessary to supplement these theories with empirical relations derived from experiments.

The case of the turbulent flow over a rough flat plate is a still more complicated phenomenon and very little work has been done in this direction in the past. Hence, the necessary empirical relations are to be derived from pipe-flow measurements. Moreover, methods of dealing with turbulent flows along a flat plate or any stream-lined body can be devised only on the basis of detailed experimental results obtained from pipe flows.

The case of the turbulent flow through pipes has been investigated very thoroughly in the past because of its greater practical applicability and the ease in carrying out measurements. The results have contributed to the extension of the fundamental knowledge of turbulent flow in general.

The skin friction on a flat plate can be very advantageously calculated from the extensive data available for pipes by the use of a method due to Prandtl and Theodre Von Karman. Calculations can be made for both smooth and rough walls.

Thus a study of the works on flow through pipes with

roughness is essential to derive the necessary roughness correlations. The introduction of the roughness parameter into our problem and the necessary correlations derived from pipe-flow measurements have been presented in Chapter 2 of the thesis.

Our aim is to apply the correlations so obtained to the flat plate case and we need a solution procedure to solve the turbulent boundary layer equations with these correlations incorporated. The procedure should be general, simple, accurate and economical in computing time. A finite-difference procedure for solving the turbulent boundary layer equations due to Patankar and Spalding[12] which satisfies our requirements has been used. The details of the method have been explained in Chapter 3. The procedure is flexible to accommodate any hypothesis, and we have used the mixing-length hypothesis due to Prandtl. The details of the computations carried out to study the effects of roughness Reynolds number, Prandtl number and also the different types of roughness have also been described in Chapter 3.

Discussion of the results of the above computations and the comparison of the same with the available data have been presented in Chapter 4.

One of the main objectives of the present work was to compare our theoritical predictions with the results of the previous experiments on the flow over rough plates. However, in the absence of any available data of such experiments, it was decided to perform our own experiment and compare the

results of the same with the theoritical prediction. Thus, we had a two-dimensional wall jet on a rough surface. Sand grain roughness was used. The set up and the details of the experimental procedure have been described in Chapter 5.

One interesting set of experimental data available was that of a radial wall jet on a rough surface by Jayatillaka.[8] A brief mention of this experiment has been made in Chapter 5. Computations were carried out to compare these experimental results with the predictions by our solution procedure.

Chapter 6 discusses the results of our experiment of a two-dimensional wall jet on a rough surface and compares the same with the theoritical predictions. It also includes the comparison of the experimental results of the radial wall jet experiment by Jayatillaka[8] with our theoritical predictions.

Concluding remarks about our investigations and the scope for the future work have been presented in Chapter 7.

CHAPTER - 2

EMPIRICAL INFORMATION ABOUT WALL ROUGHNESS

2.1 Introducing the roughness parameter

Consider the flow of a fluid on a flat plate. Near the wall, the velocity in the longitudinal direction, u, is small and there exists a one-dimensional boundary layer which is known as the Couette-flow. The characteristic feature of the turbulent Couette-flow is the dependence of velocity u or any dependent variable on y, the distance in the cross-stream direction measured from the wall, only. It follows from dimensional analysis that the velocity profile is expressible by a relationship of the form:

$$u^+ = \frac{1}{k} \ln (E\, y^+) \qquad (2.1\text{-}1)$$

where the dimensionless quantities u^+ and y^+ are defined by:

$$u^+ = \frac{u}{u_\tau} \qquad (2.1\text{-}2)$$

and

$$y^+ = \frac{y\, u_\tau}{\nu} \qquad (2.1\text{-}3)$$

Here, ν is the kinematic viscosity and u_τ is called the frictional velocity given by:

$$u_\tau = \sqrt{\frac{\tau_s}{\rho}} \qquad (2.1\text{-}4)$$

where τ_s is the shear stress at the wall and ρ is the density of the fluid.

The relationship between u^+ and y^+ is modified by surface variations such as roughness and permeability. E is the parameter into which these effects can be lumped.. In the present work, we are concerned with the effects of roughness only.

For smooth surfaces, E is a constant whose value lies between 6.5 and 9. However, for rough surfaces, E is a function of the dimensionless parameter y_r^+ which is defined by:

$$y_r^+ = \frac{y_r u_\tau}{\nu} \qquad (2.1\text{-}5)$$

where y_r is the mean height of the roughness elements.

The Roughness Reynolds number is defined as:

$$R_r = \frac{y_r u_\infty}{\nu} \qquad (2.1\text{-}6)$$

where u_∞ refers to the free-stream velocity.

We can note the relationship:

$$R_r = \frac{u_\infty}{u_\tau} y_r^+ \qquad (2.1\text{-}7)$$

The dependence of E on y_r^+ varies for different types of roughness. The $E \sim y_r^+$ relations for various types of roughness derived from pipe-flow measurements will be presented in Section 2.3.

Thermal boundary layer

Again, by the Couette-flow assumptions and by the analogy between the velocity and temperature fields, the variation of the dimensionless enthalpy, h^+, can be expressed by the relationship:

$$h^+ = \sigma_t (u^+ + P) \qquad (2.1\text{-}8)$$

The dimensionless enthalpy, h^+, is expressed as:

$$h^+ = \frac{(h_s - h)\, u_\tau \rho}{J_s} \qquad (2.1\text{-}9)$$

where J_s is the heat flux through the wall.

In equation (2.1-8), σ_t is the turbulent Prandtl number and P is the resistance of the laminar sub-layer to heat-transfer on account of the laminar Prandtl number of the fluid being different from the turbulent Prandtl number. P is given by:

$$P = \int_0^\infty \frac{\sigma_{eff} - \sigma_t}{\sigma_t}\, du^+ \qquad (2.1\text{-}10)$$

where σ_{eff} refers to the effective Prandtl number. It can be noted that,

$$\sigma_{eff} \rightarrow \sigma \quad , \text{ when } y \rightarrow 0$$
$$\text{and} \qquad \sigma_{eff} \rightarrow \sigma_t \quad , \text{ for } y \gg 0 \qquad (2.1\text{-}11)$$

The influence of roughness on the heat transfer is to be introduced through a modification of P, which gives it a dependence on the roughness. For smooth surfaces, P is a function of the ratio of the laminar to the turbulent Prandtl number only, and from pipe flow measurements, we have, for smooth surfaces

$$P = 9.24\, (\sigma / \sigma_t - 1)\, (\sigma / \sigma_t)^{-0.25} \qquad (2.1\text{-}12)$$

For rough surfaces, however,

$$P = P\{\sigma/\sigma_t, y_r^+\} \qquad (2.1\text{-}13)$$

Now, we have seen how the effect of roughness can be introduced in our problem. Our next task is to collect the $E \backsim y_r^+$ and $P \backsim y_r^+$ or $P \backsim E$ relationships for various types of roughness which we shall do so in the next sections.

2.2 Types of roughness

Roughness elements are available in various sizes, shapes and distributions. As such, their classification is slightly complicated. However, we can attempt to classify the various types according to their appearance.

Roughness types may be broadly classified into two groups, namely, regular and irregular. In the first category, all the elements are identical in shape and size and distributed according to a definite pattern. The roughness produced by knurling and machining of threads belong to this group. In the second category, the roughness elements though identical have different sizes. An example of this type is the roughness formed by sand grains having various sizes.

We can also make a distinction between two-dimensional and three-dimensional roughnesses. The roughness formed of elements which are ridges of grooves having uniform cross-section and placed at right angles to the flow belongs to the two-dimensional type and the one formed of discrete lumps or cavities belongs to the three-dimensional variety.

Another aspect of distinguishing is to observe whether

the roughness elements are packed together closely or distributed.

Now, let us consider the $E \backsim y_r^+$ and $P \backsim E$ relationships for the various types of roughness. It may be recalled here that these relationships are derived from pipe-flow measurements.

2.3 $E \backsim y_r^+$ and $P \backsim E$ characteristics

2.3-1 Uniform roughness

Our attention is devoted here to the simplest type of roughness. That is, roughness formed of elements which are uniform in size and packed as closely as possible. The roughness size, in this case, can be characterised by one particular dimension, usually the height of the elements. The following types come under this group.

Nikuradse's sand grain roughness

From the sand grain roughness data of Nikuradse[11], the $E \backsim y_r^+$ relationship for the fully rough region is given by:

$$E = \frac{\beta}{y_r^+} \qquad (2.3\text{-}1)$$

where β is a constant of the order 30. The fully rough region is defined by $y_r^+ > \beta / E_M$, where E_M denotes the value of E for the smooth surface. For the hydrodynamically smooth region,

$$E = E_M \qquad (2.3\text{-}2)$$

The $P \sim E$ characteristic for the sand grain roughness from the measurements of Dipprey and Sabersky[6] is given by:

$$P = 3.15 \left(\sigma / \sigma_t \right)^{0.695} \left(1/E - 0.1111 \right)^{0.259} + 0.267 \, E^{0.6} \, P_H \qquad (2.3\text{-}4)$$

Here, P_H denotes the value of P for the hydrodynamically smooth region given by the equation (2.1-12).

Cope's pyramidal roughness

Pyramidal type roughness has been studied by Cope[5] and Stamford[16]. Cope used the whole pyramids while Stamford considered truncated cones. The roughness characteristics are given by:

$$E = \frac{\beta}{y_r^+} \qquad (2.3\text{-}5)$$

and

$$P = 62.1 \left(\sigma / \sigma_t \right)^{0.695} E^{-0.359} \qquad (2.3\text{-}6)$$

In this case, the constant β is of the order 13.

Kolar's V - groove roughness

The relations for E and P for the V-groove type of roughness can be derived from the experimental investigations of Kolar[9].

2.3-2 Natural roughness

Natural roughness arises in commercial steel, wrought iron and galvanised iron pipes and such things due to slight

waviness and surface irregularities left during machining processes and other unknown causes. In this case, we cannot define the roughness height as in the case of uniform roughness. However, we can use what is generally known as the 'equivalent sand roughness height'.

Colebrook[4] has suggested the following relationship:

$$E = \frac{34.02}{y_r^+ + 3.305} \qquad (2.3\text{-}7)$$

P-values derived from experimental results for the galvanised iron and steel pipes do not show a systematic difference between these types of material, and hence a general relationship for P has not been evaluated.

2.3-1 Distributed roughness

In the case of distributed roughness, the elements are distributed over the surface with areas of smooth surface interspread. As such, the $E \backsim y_r^+$ and $P \backsim E$ characteristics vary significantly from those of closely packed type.

Roughness formed by wires stretching at right angles to the flow

The $E \backsim y_r^+$ characteristic derived from the data of Malherbe[10] is given by:

$$E = 38.0\ (0.0362/y_r^+)^{1/\exp\ (0.123\ +\ 0.0082\ p_r/y_r)} \qquad (2.3\text{-}8)$$

where p_r is the spacing of the wires and y_r, the roughness height. The above relationship is valid when $p_r/y_r < 6.25$ and $20 < y_r^+ < 200$.

Roughness formed due to ridges with square cross-section

From the drag data correlation of Bettermann[2], we have:

$$E = \frac{8.0}{y_r^+} \exp\left[6.94 - 4.9 \ln\left(p_r/y_r\right)\right] \qquad (2.3\text{-}9)$$

which is valid when $180 < y_r^+ < 750$ and $2.7 \leq p_r/y_r \leq 4$.

Square thread type roughness

The roughness characteristics for square thread type roughness can be derived from the data of Sams[14].

Three-dimensional distributed roughness

Some data available on this type of roughness are due to Ambrose[1] who used pipes roughened with small circular cylindrical projections and with cylindrical cavities, and due to Doenecke[7] who made experiments on a plate with short cylindrical projecting elements.

This concludes the collection of the necessary correlations. Our next aim is to solve the turbulent boundary layer equations incorporating these correlations in the wall region. We shall use a finite-difference procedure due to Patankar and Spalding[12], the details of which we shall explain in the next chapter.

CHAPTER - 3

THE SOLUTION PROCEDURE

3.1 Introduction

The conventional finite-difference procedure is known to be conceptually simple and accurate, but very expensive in computing time. However, the new procedure developed by Patankar and Spalding[12] incorporates devices which reduce the computing time to a very large extent, but at the same time retain the advantages of the finite-difference method.

The novel features of this method are the use of a grid that always adjusts its width so as to conform to the thickness of the layer, and the use of the Couette-flow relationships near a wall. These features have brought about a substantial saving in the computing time.

The procedure is very general and is applicable to all kinds of boundary layers: free, external, confined, wall-jets etc. The method can also handle cases of variation of pressure gradient, mass transfer, fluid density, wall temperature etc.

We shall explain in the sections below how the method can be applied to our present study.

3.2 The conservation equations

The boundary layer is considered to lie between two imaginery surfaces for which the subscripts I (internal) and E (external) will be used. The conservation equations are

written in the (x, ψ) co-ordinate system. The stream function is defined by:

$$x\text{-fixed;} \qquad d\psi = \rho u r \, dy \tag{3.2-1}$$

The advantages of using the (x, ψ) co-ordinate system are that the continuity equation is automatically satisfied and the reduction in the number of terms.

The conservation equations in the $x \sim \psi$ co-ordinates system are:

conservation of momentum in x-direction:

$$\frac{\partial u}{\partial x} = \frac{\partial}{\partial \psi} (\tau r) - \frac{1}{\rho u} \frac{dp}{dx} \tag{3.2-2}$$

conservation of stagnation enthalpy:

$$\frac{\partial \tilde{h}}{\partial x} = - \frac{\partial}{\partial \psi} \left[(J - u\tau) r \right] \tag{3.2-3}$$

The shear stress and heat flux are expressed through effective exchange coefficients, and we have the following exchange laws:

$$\tau = \mu_{eff} (\partial u / \partial y) \tag{3.2-4}$$

$$J = - \frac{\mu_{eff}}{\sigma_{eff}} (\partial h / \partial y) \tag{3.2-5}$$

The effective viscosity is evaluated from Prandtl's mixing length hypothesis:

$$\mu_{eff} = \rho \, l^2 \left| \partial u / \partial y \right| \tag{3.2-6}$$

where l is the mixing length. Escudier has recommended the following variation for l :

$$\begin{aligned} \ell &= k\,y \quad ; \quad 0 < y \leq \lambda y_\ell / k \\ \ell &= \lambda\, y \quad ; \quad \lambda y_\ell / k < y \end{aligned} \qquad (3.2\text{-}7)$$

where λ and k are constants, and y_ℓ is a characteristic thickness of the layer. Jayatillaka[8] has recommended a value of 0.9 for the effective Prandtl number.

The stagnation enthalpy is given by:

$$\tilde{h} = h + \frac{u^2}{2} \qquad (3.2\text{-}8)$$

where h is the specific enthalpy.

3.3. Initial profiles of velocity and temperature

To solve the boundary layer equations, it is necessary to know the profiles of the dependent variables at a station upstream of the region of interest. We have used a power-law relationship for both the velocity and temperature. These profiles are generated through the prescription of shape factor and momentum Reynolds number.

3.4 Boundary conditions

The solution procedure needs the information along the boundaries. The boundary conditions are:

$$\begin{aligned} &\text{At the wall,} \quad u = 0 \quad \text{and} \quad T = T_s \\ &\text{At the free stream ,} \quad u = u_\infty \text{ and } T = T_\infty \end{aligned} \qquad (3.2\text{-}9)$$

3.5 The region near the wall

The region near the wall is very important in our analysis and needs special treatment; the reasons being that usually very steep gradients of velocity and other variables

exist in this region and that the shear stress and fluxes at the wall are of great practical interest. In the present problem, we deal with this region with our logarithmic velocity distribution mentioned in Section 2.1. Now, we shall see how we can calculate the shear stress and the heat flux at the wall using the roughness correlations and the logarithmic velocity distribution.

3.5-1 Shear stress at the wall

The dimensionless shear stress at the wall is defined by:

$$s = \frac{\tau_s}{\rho u^2} \qquad (3.5\text{-}1)$$

From the definition of u^+, the above relationship can be written in the form:

$$u^+ = \frac{1}{\sqrt{s}} \qquad (3.5\text{-}2)$$

The Reynolds number can be expressed as:

$$R = u^+ y^+ \qquad (3.5\text{-}3)$$

Hence, equation (2.1-1) can be written as:

$$\frac{1}{\sqrt{s}} = \frac{1}{k} \ln (E R \sqrt{s}) \qquad (3.5\text{-}4)$$

The dimensionless shear stress s is evaluated from the equation (3.5-4) by an iterative procedure after substituting the appropriate $R \sim y_y^+$ relationship for the particular type of roughness considered.

The shear stress at the wall is then given by:

$$\tau_s = \rho\, u^2\, s \qquad (3.5\text{-}5)$$

The skin-friction coefficient C_f is calculated from the relation:

$$\frac{C_f}{2} = \frac{\tau_s}{\rho\, u_\infty^2} \qquad (3.5\text{-}6)$$

3.5-2 Heat flux at the wall

The dimensionless heat flux at the wall is defined by:

$$S = \frac{J_s}{\rho\, u\, (h_s - h)} \qquad (3.5\text{-}7)$$

where J_s is the heat flux through the wall.

From the definitions of h^+ and u^+, the above relationship can be expressed in the form:

$$S = \frac{1}{h^+ u^+} \qquad (3.5\text{-}8)$$

Substituting for h^+ from the equation (2.1-8), we get:

$$S = \frac{1}{\sigma_t\, u^+ (u^+ + P)} \qquad (3.5\text{-}9)$$

S is calculated from the equation (3.5-9) after substituting the appropriate correlation for P. It can be noted that u^+ has already been calculated while evaluating the shear stress, s.

The Stanton number is then calculated from the relation:

$$St = \frac{J_s}{\rho\, u_\infty (h_s - h_\infty)} \qquad (3.5\text{-}10)$$

This concludes the treatment of the one-dimensional region near the wall. A one-dimensional region, however, does not exist in the outer parts of the boundary layer. The conservation equations there are solved by the finite-difference method. We shall see in the section below the details of this procedure.

3.6 The finite-difference solution

3.6-1 The co-ordinate system

The co-ordinate system forms an important aspect of a finite-difference procedure. With the usual (x,y) co-ordinate system, the computing time becomes excessively large. The same is the case with the (x, ψ) system also. An ideal system will be to have a grid which always fits the boundary layer region. The Patankar-Spalding procedure employs a grid which always fits the regions of flow where the dependent variables vary significantly, through the use of a dimensionless stream function as the cross-stream variable and an appropriate formula for the mass transfer rate across the free boundary which is also known as the entrainment rate. This novelty has brought about a substantial saving in the computing time, at the same time maintaining high accuracy at all stations.

The dimensionless stream function is defined by:

$$\omega = \frac{\psi - \psi_I}{\psi_E - \psi_I} \qquad (3.6\text{-}1)$$

It can be seen that the boundary layer is always enclosed in the region between $\omega = 0$ and $\omega = 1$.

3.6-2 Conservation equations in $x \sim \omega$ co-ordinate system

The conservation equations of section 3.2 are transferred to the $x \sim \omega$ system, and they possess the common form:

$$\frac{\partial \phi}{\partial x} + (a + b\omega)\frac{\partial \phi}{\partial \omega} = \frac{\partial}{\partial \omega}\left(c \frac{\partial \phi}{\partial \omega}\right) + d \qquad (3.6\text{-}2)$$

where ϕ stands for the dependent variable and d is the term which does not contain $\partial\phi / \partial\omega$.

3.6-3 The difference equation

The conservation equations are expressed in a finite-difference form, and solved by step-by-step forward integration.

The discrete values of ω decided before hand define a grid; a portion of this is shown in Figure 3.6-1.

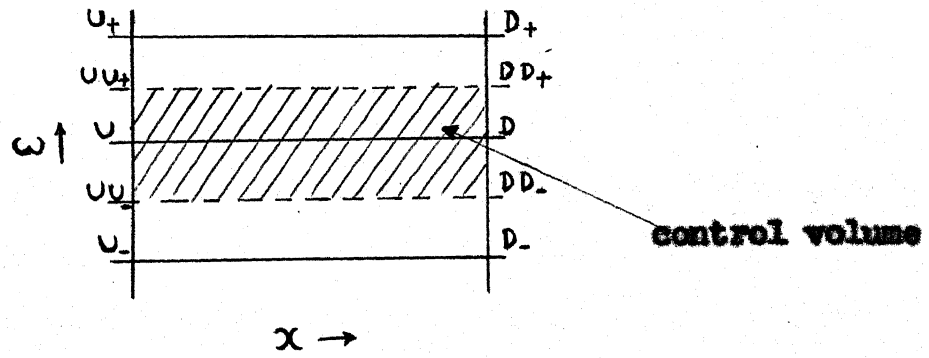

Fig. 3.6-1

The four midway points UU_+, DD_+, UU_- and DD_- form the control volume, which is used in forming the difference equation. The finite-difference equation is obtained by expressing each term in the conservation equation as an integrated average on the control volume. It is assumed that between grid points, the variation of the dependent variable ϕ is linear in ω. With these general principles, after expressing the individual terms in the conservation equation in the finite-difference form, the complete difference equation reduces to the form:

$$\phi_D = A\,\phi_{D_+} + B\,\phi_{D_-} + C \qquad (3.6\text{-}3)$$

3.6-4 Solution of the difference equation

A difference equation is obtained for every grid line, and thus a set of linear algebraic equations are formed. These equations are solved by simple successive-substitution formulae.

3.6-5 Determination of step length

The size of the forward step is chosen such that the quantity of the fluid entrained during the step would be a certain percentage of the amount of the fluid already existing in the layer. The implicit nature of the finite-difference scheme ensures stability even for large steps.

3.7 Computations

A computer programme based on the solution procedure has been formulated. The necessary computations can be carried out through proper modifications.

Computations were carried out to study the following two types of roughness:

(i) Nikuradse's sand grain roughness

(ii) Cope's pyramidal roughness.

Computations were carried out for Roughness Reynolds numbers of 10, 100, 300, 1000, and 3000. Computations were carried out to study the effects of Prandtl number. The following Prandtl numbers were considered: 0.7, 1.0, 30, 100 and 1000. Quantities like skin friction coefficient, Stanton number, momentum Reynolds number, shape factor etc. were computed and printed after every five integrations. The range of computation was from R_x equal to 1.7×10^4 to 1.2×10^7.

We shall present and discuss the results of our computations in the next chapter.

CHAPTER - 4

RESULTS AND DISCUSSIONS

4.1 Hydrodynamic boundary layer

4.1-1 Velocity profiles

Figures 4.1-1 and 4.1-2 show a set of velocity profiles plotted on a non-dimensional basis. It can be seen that the velocity gradient becomes steeper with an increase in the Roughness Reynolds number. This indicates an increase in the shear stress with an increase in the height of the roughness elements. The same trend is observed in both the sand grain and pyramidal types of roughness.

4.1-2 Variation of E

Figures 4.1-3 and 4.1-4 show a plot of E against R_x, the plate Reynolds number, for different Roughness Reynolds numbers. It is observed that the surface behaves as hydrodynamically smooth at very low Roughness Reynolds numbers; in other words, when the height of the roughness elements is small. Also, at high Roughness Reynolds numbers, the surface tends towards hydrodynamic smoothness with the increase in the plate Reynolds number. This is obvious, since the thickness of the laminar sub-layer increases with the downstream distance, and the height of the roughness elements becomes smaller when compared with the thickness of the sub-layer. Consequently, the skin friction decreases downstream.

4.1-3 Effect of roughness on the skin friction

Figure 4.1-5 shows the skin friction coefficient on a smooth surface plotted against the plate Reynolds number. It can be seen that the agreement is satisfactory when compared with the Spalding and Chi[3] correlation for flat-plate drag.

Figures 4.1-6 and 4.1-7 show the effects of the Roughness Reynolds number on the skin friction. It can be seen that the skin friction increases with the increase in the Roughness Reynolds number.

4.2 Thermal boundary layer

4.2-1 Temperature profiles

Temperature profiles for different Roughness Reynolds numbers, for the case of the sand grain roughness are shown in Figures 4.2-1 and 4.2-2. It can be observed that, similar to the velocity profile, the temperature profile also becomes steeper with the increase in the Roughness Reynolds number. The same trend follows at higher Prandtl numbers also.

4.2-2 Effect of roughness on the Stanton number

Figure 4.2-3 shows the variation of the plate Stanton number on a smooth surface. The effect of the Roughness Reynolds number on the plate Stanton number in the case of sand grain roughness is shown in Figure 4.2-4. It can be seen that the Stanton number increases with the increase in the Roughness Reynolds number, or in other words, with the height of the roughness elements.

4.2-3 Effect of Prandtl number

Figure 4.2-5 shows the effect of increasing the Prandtl number on the Stanton number for various Roughness Reynolds numbers. The Stanton number on a plate decreases with increasing Prandtl number on both smooth and rough surfaces. This is obvious since the thermal conductivity decreases. Also, at large Prandtl numbers the effect of the plate Reynolds number is small. We have seen that the Stanton number increases with the Roughness Reynolds number. However, it can be noticed that at very large Prandtl numbers, the effect of Roughness Reynolds number is small.

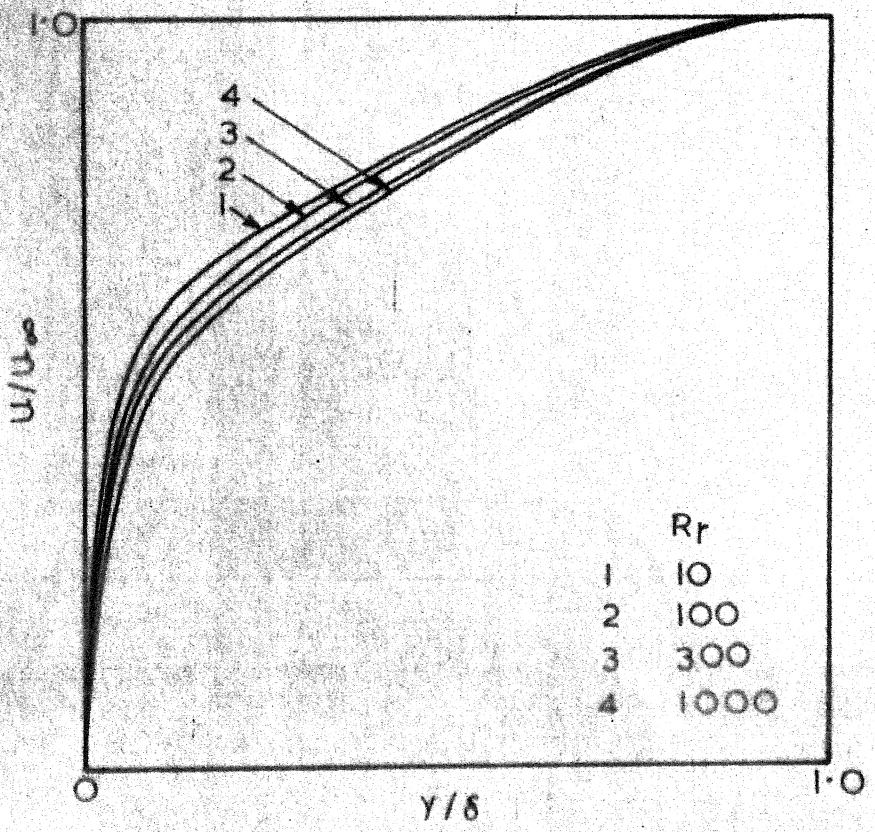

FIG. 4·1-1 VELOCITY PROFILES (SAND GRAIN ROUGHNESS)

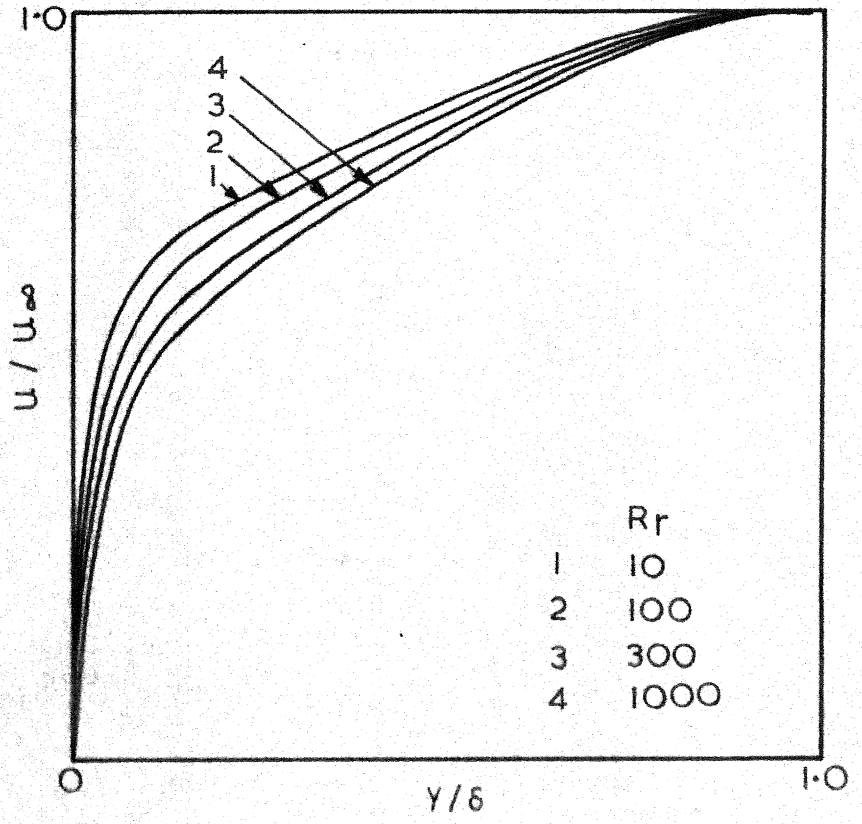

FIG. 4·1 2 VELOCITY PROFILES (PYRAMIDAL ROUGHNESS)

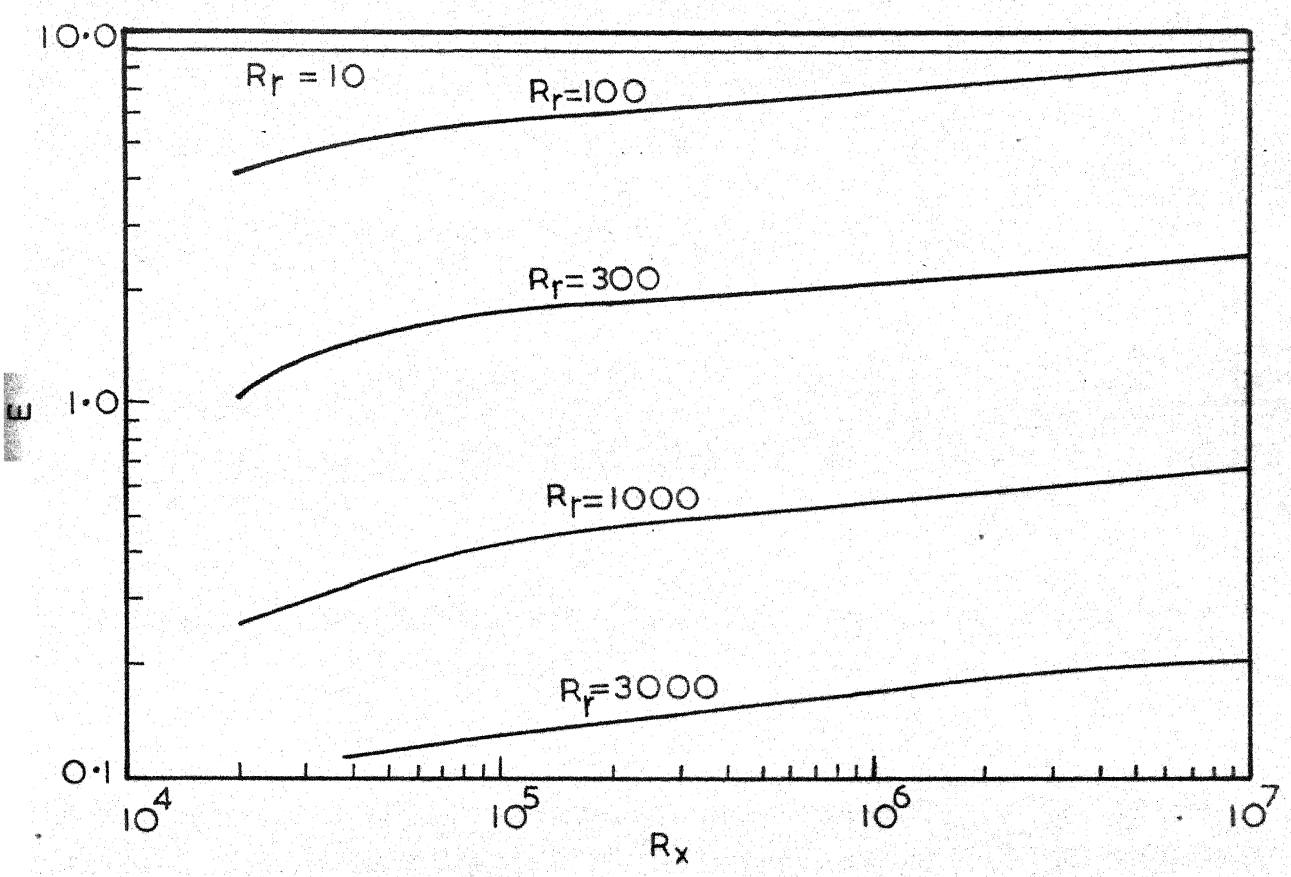

FIG. 4·1-3 VARIATION OF E (SAND GRAIN ROUGHNESS)

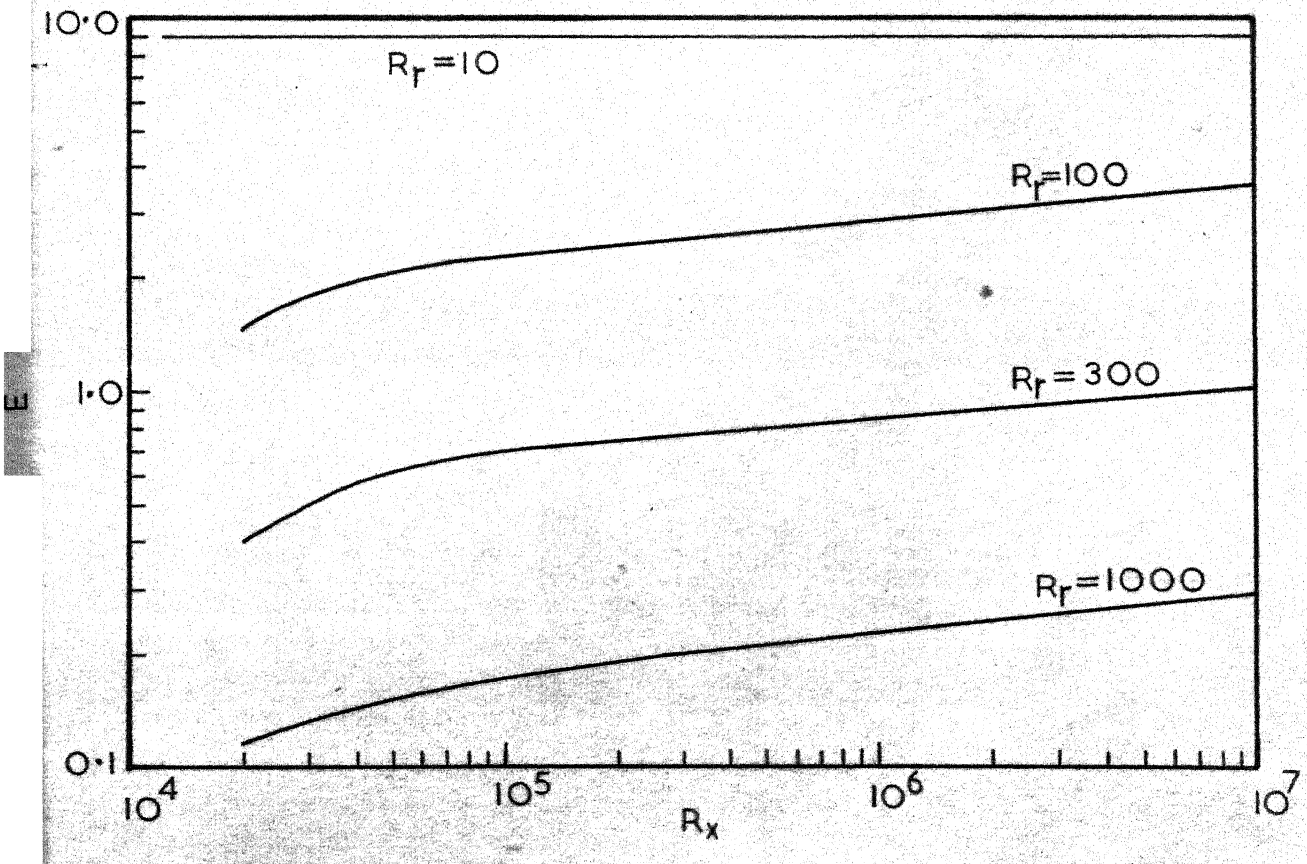

FIG. 4·1-4 VARIATION OF E (PYRAMIDAL ROUGHNESS)

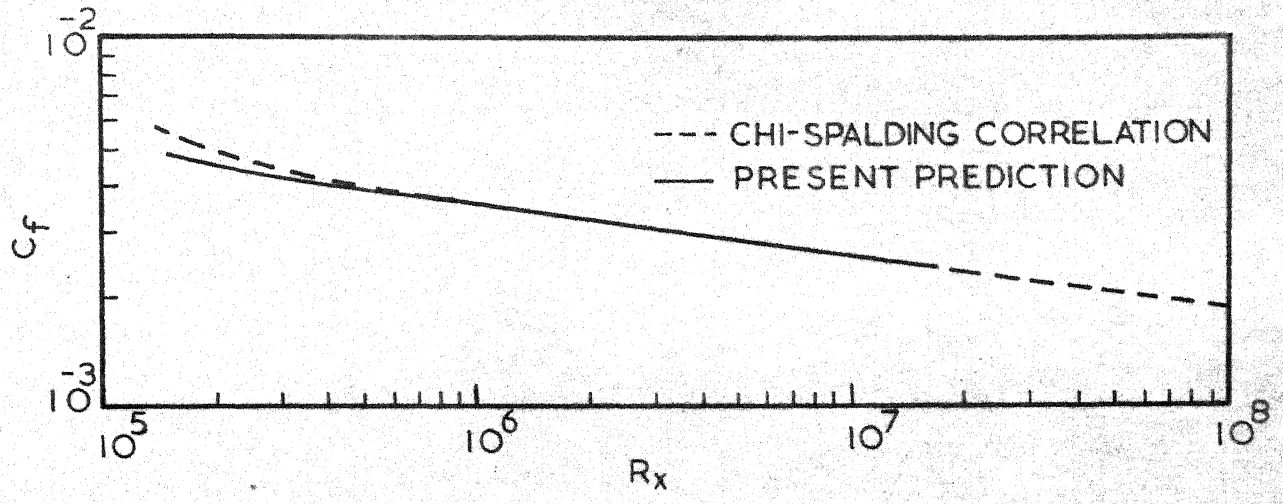

FIG. 4·1-5 SKIN FRICTION ON A FLAT PLATE

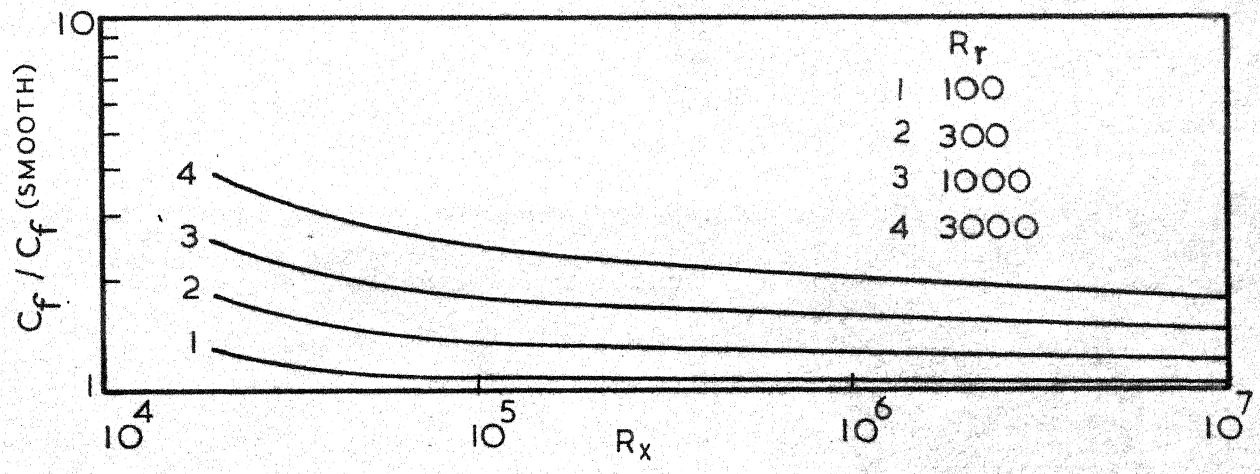

FIG. 4·1-6 EFFECT OF ROUGHNESS ON SKIN FRICTION (SAND GRAIN ROUGHNESS)

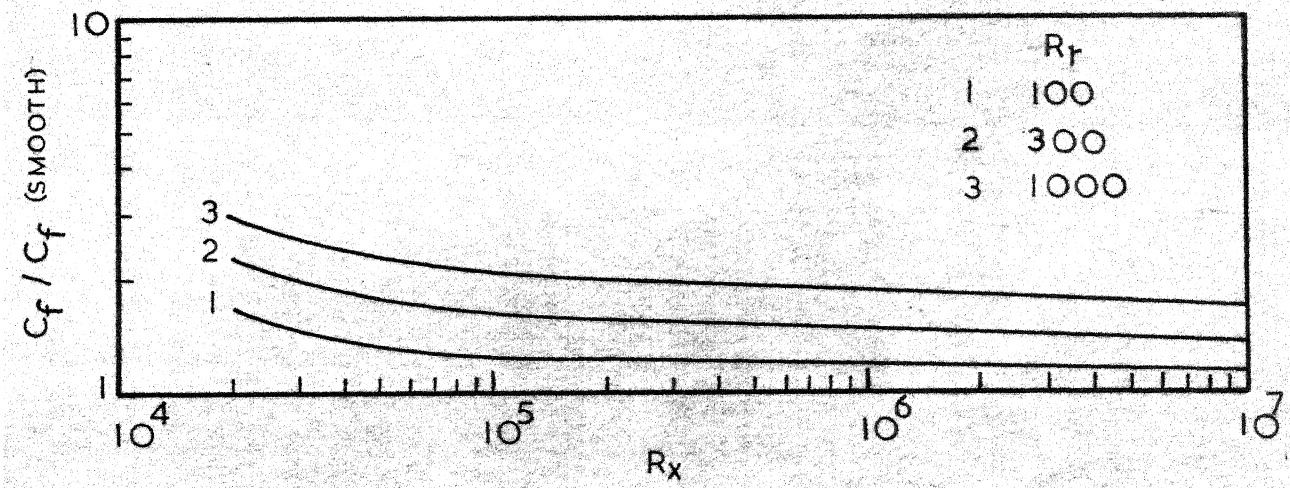

FIG. 4·1-7 EFFECT OF ROUGHNESS ON SKIN FRICTION (PYRAMIDAL ROUGHNESS)

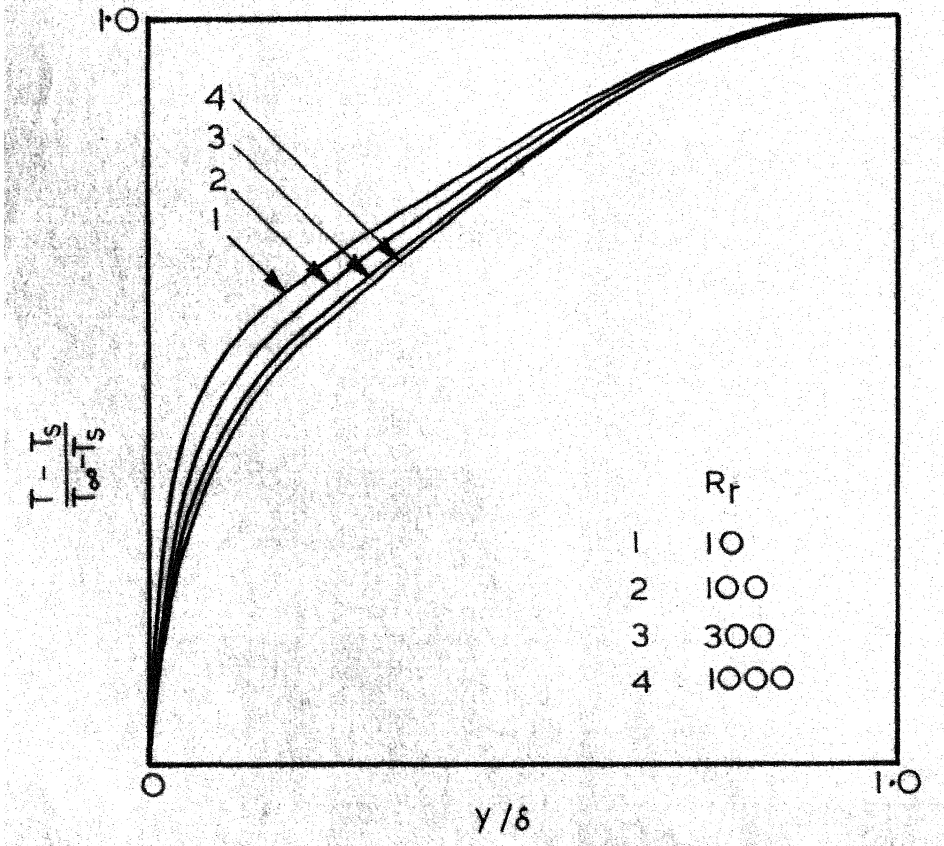

FIG. 4·2-1 TEMPERATURE PROFILES
(PRANDTL NUMBER=0·7)

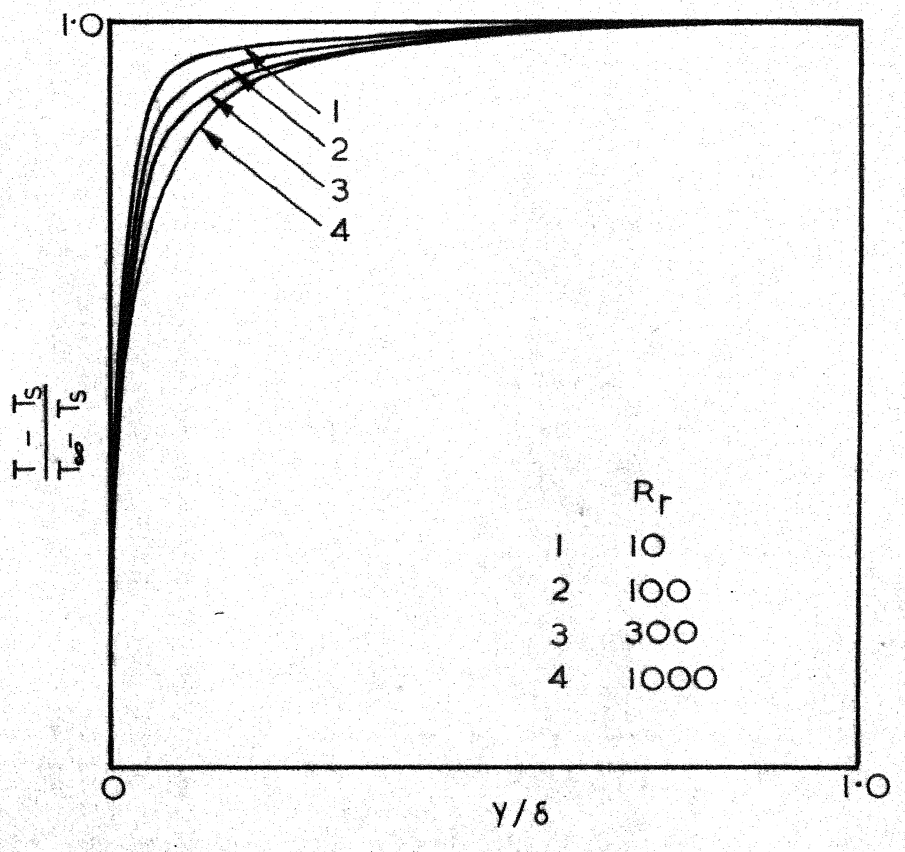

FIG. 4·2-2 TEMPERATURE PROFILES
(PRANDTL NUMBER=1000)

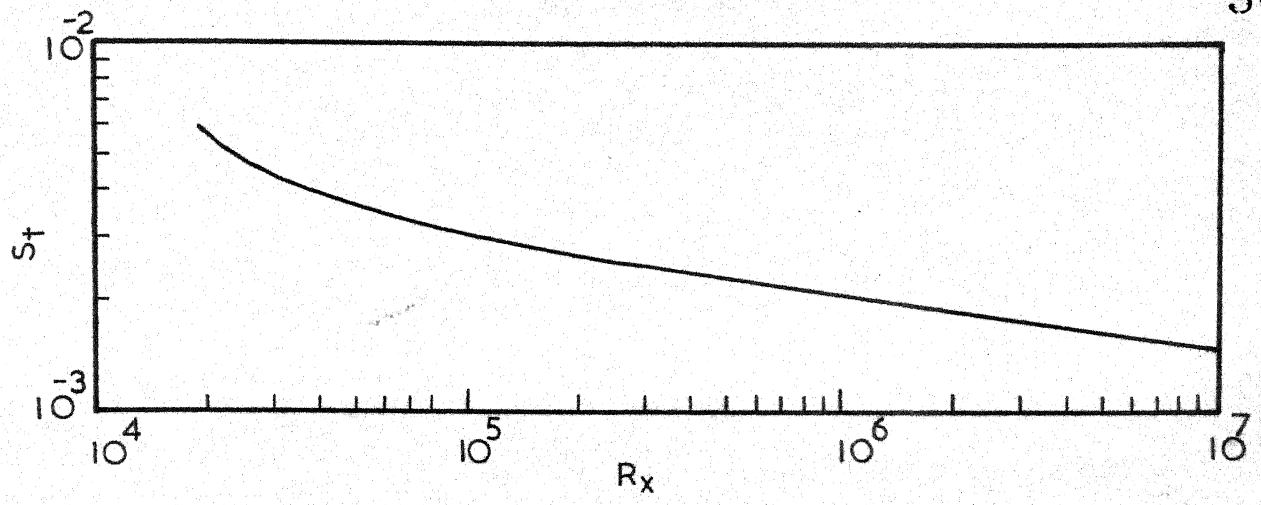

FIG. 4·2-3 STANTON NUMBER ON SMOOTH SURFACE

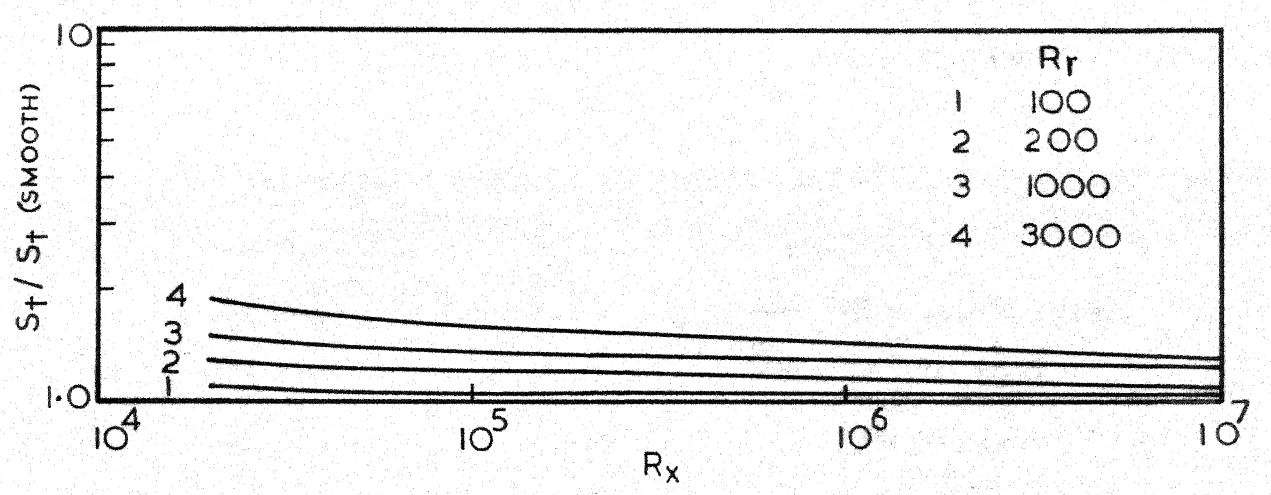

FIG. 4·2-4 EFFECT OF ROUGHNESS ON STANTON NUMBER

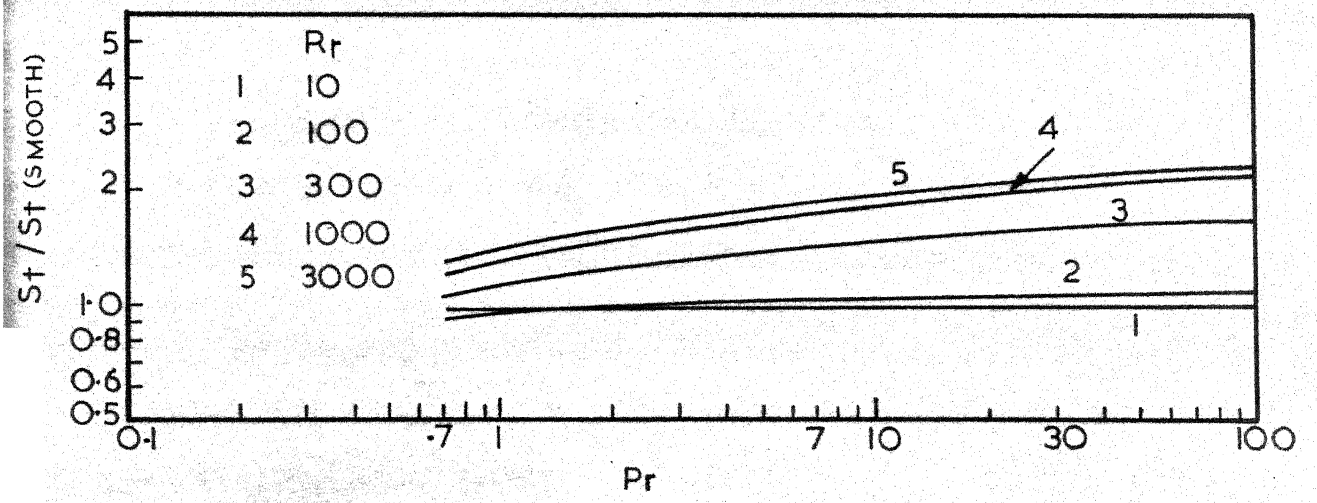

FIG. 4·2-5 EFFECT OF PRANDTL NUMBER

CHAPTER - 5

EXPERIMENTAL INVESTIGATION

5.1 Purpose and outline of the experiment

The need for the experimental work has been explained in section 1.2. The primary object is to obtain experimental data to be compared with our theoretical predictions, and see how the two agree with each other.

Experiments were conducted to study the flow developments in a plane wall jet on a rough surface. This was considered to be an interesting problem since the effects of wall roughness have not been investigated. Sand grain roughness was used.

Experimental data are here obtained for the velocity profiles in the absence of mass transfer through the wall. Measurements of jet growth and velocity decay are made. The wall jet thickness increases and the velocities decay with the increase in the distance from the slot; and in the case of a surface with uniform height of roughness, this would amount to a change in the roughness Reynolds number with the downstream distance from the slot.

The system used is schematically shown in the Figure 5.3-1. The fluid used was air. The rough plate consisted of a 'perspex' sheet with sand papers pasted on its surface.

5.2 Choice of roughness

The following factors influenced the choice of roughness type used for the experiments:

(i) availability of the $E \backsim y_r^+$ characteristic for the prediction of hydrodynamic aspects.

(ii) availability of the rough surface itself.

Though $E \backsim y_r^+$ characteristics are available for different types of roughnesses, namely, sand grain roughness, pyramidal roughnesses of Cope and Stamford, Kolar's V-groove roughness etc., the second factor, namely, the availability influenced to a great extent in selecting the type of roughness for the experiments. Sand grain roughness was selected, since sand papers were easily available and the $E \backsim y_r^+$ characteristic for the sand roughness could be used.

Three different grades of sand paper, namely, '1', '1½' and '2' were used. The thickness of the grains were measured using a travelling microscope and the mean height of the grains were found to be 0.13, 0.31 and 0.37 mm respectively.

5.3 Description of the apparatus and instrumentation

The arrangement of the apparatus is shown in Figure 5.3-1. Air from the blower is conducted through a closed galvanised-iron duct and injected along the plate placed in a rectangular wooden channel through the uniform gap formed between two flat pieces of perspex sheet at the end of the delivery system. We shall refer to the gap through which air is blown as the 'slot'.

Experiments were conducted on both smooth and rough surfaces. For each surface, experiments were repeated for different slot heights and flow rates.

Velocities were measured with a Pitot tube connected to an inclined manometer which read the dynamic pressure in inches of water.

5.3-1 Blower and delivery system

A centrifugal fan* was used to provide the air. The fan coupled to an A.C. motor was mounted on a rigid base. The duct carrying the air to the plate was securely connected to the blower. The duct had an opening in it through which a plate could slide, so that by varying the position of the plate, the flow rate could be varied.

5.3-2 The slot

The slot was made of two perspex sheets of size 50.5 x 4.5 x 1.0 cms. Effective slot width was 43.8 cms. The lower piece was glued to the base of the channel in flush with it and the upper piece was connected to the air duct through a thick flexible paper passage. Screwed rods with knobs at the tops passed through bushes in the plates. By operating the knobs, the upper plate could be raised or lowered, thus enabling slot height variation.

5.3-3 The plate

A 'perspex' sheet 95.5 x 52.8 cms. in dimensions and 1 cm thick was used for smooth surface runs. Sand papers were glued on the surface of the sheet using adhesive tapes for rough surface runs.

---

* Speed - 1435 R.P.M
Capacity - 1463 cubic feet/minute.
H.P. - 0.348

The plate was placed in the rectangular wooden channel and screwed to its base. The channel was mounted on a rigid platform.

5.3-4 Instrumentation

The Pitot tube

Dynamic pressures were measured with a circular Pitot probe of diameter 1.76 mm. The smaller side of the probe was 5.5 cms long and bent at an angle of 95° aproximately. The longer side of the probe passed through a tube 17 cms long and 3/8 inches in diameter, and firmly secured in it. The tube in turn was held firmly in the traversing mechanism. The other end of the tube was connected to an inclined manometer through plastic tubing.

The traverse unit

Velocity profiles were measured at different stations along the plate. At each station, the characteristic thickness of the boundary layer was also measured. Hence, it was necessary for the probe to be moved along the length of the plate and also in the verticle direction. It was also needed to move the probe in the cross-wise direction to check the two-dimensionality of the flow.

The traverse unit consisted of a brass square plate mounted on which was a graduated rod. The rod carried an arm to which the steel tube carrying the probe was secured by means of a set-screw. The tube and hence the probe could be raised or lowered by actuating a micrometer head. It could be located with an accuracy of 0.5 mm.

The unit was placed on a frame work formed of angle irons placed across the channel, atop it. The unit could be moved across the channel on this frame work and fixed at any desired position. The frame work with the traverse unit itself could be moved along the length of the channel and fixed at any desired station. The position could be marked using the scale attached to the channel. Spring-clips were used to hold the probe firmly, without vibrations, during the experiments.

Manometer

Velocity profiles were measured using an inclined manometer which read the dynamic pressures in inches of water. A red fluid of specific gravity 0.88 was used. The manometer could read upto 0.02 inches of water.

5.4 The experimental procedure

5.4-1 Setting the slot height

An important part of the work before the actual running of the tests was setting up the slot height. The aim was to obtain the required slot height and have it as uniform as possible over the entire width of the plate.

The slot was adjusted aproximately to the desired height by operating the knobs and using the scale attached to the side of the channel. The blower was started. The probe was positioned in the centre of the channel and the height of the probe above the surface was adjusted exactly to the desired value of the slot height. The position of the probe was adjusted

by trial and error till it was parallel to the direction of the flow. Now, the probe was placed just infront of the slot and the knobs were operated till the manometer read zero velocity pressure. The uniformity of the slot was tested by positioning the probe at different points along the width of the slot and making finer adjustments till the manometer read zero velocity pressure at all positions of the probe. The slot height was tested often to ensure that it remained uniform throughout the experiment.

5.4-2 Velocity profiles

Velocity profiles were measured at the centre of the plate. The blower was started and the jet was allowed to work for a few minutes to reach steady state conditions. The velocity profile measurements were then commenced, the first station being the slot itself. To start with, the probe was flushed against the surface, taking care to see that the probe just touched the surface and did not bend due to excessive pressure. The manometer reading was noted. Then the micrometer head was rotated to displace the probe by 0.5 mm each time and the manometer reading noted. The 0.5 mm movement was continued for about ten more readings.

The profile was completed by taking readings with the probe at various positions with smaller spacings near the surface and increased spacings once the maximum velocity point was passed, till the manometer read zero velocity pressure.

The probe was then removed from the slot and velocity profiles were measured at 4 stations downstream. The first two

stations were chosen near the slot, and the remaining stations at progressively increasing spacings between each other.

After the velocity profiles were completed, the spread of the jet was measured. For this purpose, readings were taken at ten stations downstream of the slot, the stations being spaced progressively increasing between each other. At each station, the maximum velocity and the thickness of the layer, $y_{\frac{1}{2}}$, where the velocity was half the maximum velocity were measured.

Now, the flow rate was changed and the complete set of operations repeated. Experiments were repeated for four flow rates for each slot setting.

Next, the slot height itself was changed and the experiments repeated. Three slot heights, 3 mm, 6 mm and 12 mm were used.

The entire set of operations was conducted on the three grades of rough surface and also on the smooth surface. For each surface, there were three slot settings with four flow rates for each setting. Altogether 48 sets of readings were taken.

The measurements of velocity profile and the spread of the jet on both the smooth and rough plates are given in Tables 5.4-1 to 5.4-8 for typical slot Reynolds numbers. The slot Reynolds number is calculated from

$$\text{slot Reynolds number} = \frac{y_c \, u_c}{\nu}$$

where y_c is the height of slot opening, u_c is the velocity at

the slot and ν, the kinematic viscosity of the fluid.

We shall present the results of our experimental investigation in the next chapter and see how they agree with the theoretical predictions.

5.5 Radial wall jet

Jayatillaka[8] has conducted experiments on the flow development and heat transfer in a radial wall jet on a rough surface.

The experimental set-up consisted of a jet issuing out of a nozzle and spreading radially on a flat plate. Experiments were conducted on two types of rough surfaces and also on the smooth surface. The roughness types considered were emery roughness and V-groove type of roughness. Experiments were repeated for different slot heights in each case. Velocity and temperature measurements were made at different stations along the surface.

For the purpose of comparison, we have considered the flow development part only. Comparisons have been made for the smooth and emery roughness cases. Results of these comparisons shall be presented in the next chapter.

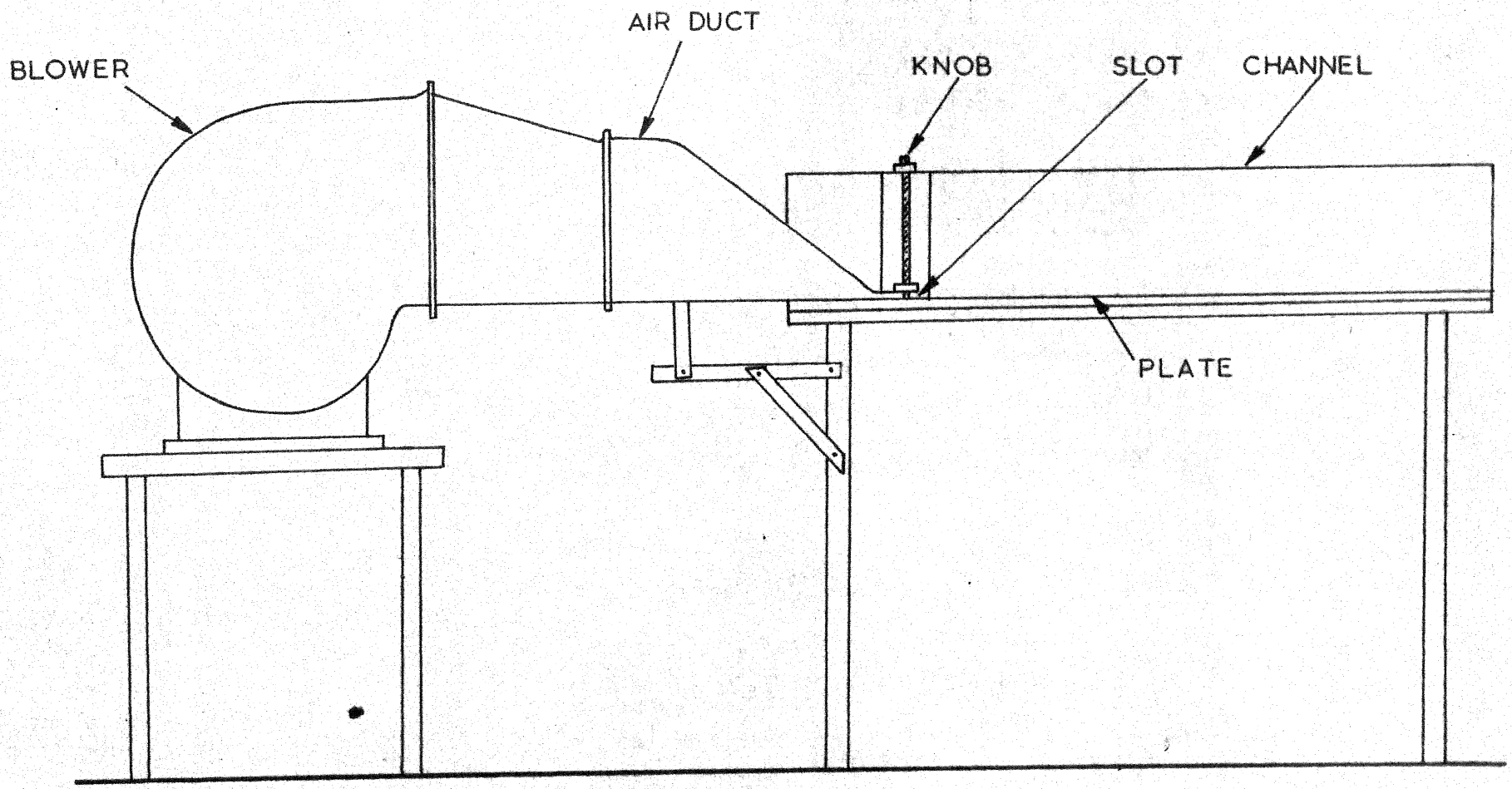

FIG. 5-3-1 GENERAL ARRANGEMENT OF THE EXPERIMENTAL SET-UP

Table 5.4-1 (a)

Velocity profile data

Smooth surface. Slot opening = 6 mm. Slot Re = 1.020×10^4

x = 0		x = 1.97"		x = 3.94"		x = 7.88"	
y inches	u ft/sec	y inches	u ft/sec	y inches	u ft/sec	y inches	u ft/sec
0.034	82.08	0.034	75.51	0.034	63.68	0.034	46.77
0.053	82.54	0.053	77.52	0.053	65.61	0.053	47.30
0.072	83.00	0.072	79.62	0.072	67.45	0.072	49.55
0.091	82.54	0.091	99.62	0.091	67.05	0.091	50.50
0.110	82.40	0.110	78.54	0.110	66.04	0.110	50.90
0.129	82.08	0.129	76.41	0.129	65.05	0.129	50.92
0.148	81.50	0.148	73.63	0.148	63.49	0.148	50.92
0.167	81.00	0.186	66.82	0.167	61.55	0.167	50.55
0.186	78.88	0.224	59.43	0.186	59.80	0.186	49.55
0.205	77.00	0.262	50.00	0.224	55.05	0.224	48.15
0.224	62.45	0.300	41.12	0.262	50.00	0.262	46.77
0.243	40.49	0.338	34.75	0.300	46.28	0.300	45.42
0.262	8.56	0.376	26.74	0.338	41.64	0.338	43.32
		0.414	20.04	0.376	36.60	0.376	41.44
		0.452	13.36	0.414	32.78	0.414	39.00
		0.471	9.45	0.452	28.19	0.490	34.75
		0.490	6.68	0.490	24.08	0.566	30.62
				0.528	20.04	0.642	25.88
				0.566	16.78	0.718	22.16
				0.604	11.58	0.794	17.67
				0.642	9.45	0.956	11.58
				0.661	6.68	1.032	6.68

Table 5.4-1 (b)

Spread of the wall jet

x inches	$y_{\frac{1}{2}}$ inches	u_{max} ft/sec	x/y_c	$y_{\frac{1}{2}}/y_c$	u_{max}/u_c
0.00	0.240	83.00	0.00	0.90	1.000
1.97	0.320	79.62	8.32	1.34	0.960
3.94	0.419	67.45	16.66	1.77	0.812
5.91	0.512	59.00	25.00	2.16	0.700
7.88	0.676	50.92	33.82	2.85	0.615
9.85	0.846	45.80	41.65	3.58	0.552
11.82	1.034	41.44	50.00	4.37	0.498
13.79	1.200	37.20	58.32	5.08	0.448
15.76	1.400	34.75	66.64	5.91	0.418
19.70	1.812	29.85	83.33	7.66	0.360
23.64	2.324	26.74	100.00	9.66	0.322

Table 5.4-2 (a)

Velocity profile data

Smooth surface. Slot opening = 12 mm. Slot Re = 2.040×10^4

x = 0		x = 1.97"		x = 3.94"		x = 7.88"	
y inches	u ft/sec	y inches	u ft/sec	y inches	u ft/sec	y inches	u ft/sec
0.034	80.50	0.034	71.05	0.034	65.05	0.034	61.95
0.053	81.50	0.053	76.50	0.053	71.35	0.053	66.50
0.072	82.40	0.072	79.82	0.072	75.00	0.072	68.50
0.091	82.80	0.091	80.95	0.091	76.50	0.091	69.76
0.110	83.22	0.110	81.50	0.110	77.98	0.110	71.05
0.129	82.80	0.129	81.80	0.129	78.54	0.129	71.35
0.148	82.80	0.148	81.82	0.148	78.88	0.148	71.58
0.186	82.80	0.167	81.80	0.167	79.00	0.167	71.58
0.224	82.54	0.186	81.64	0.168	78.54	0.186	71.58
0.262	82.40	0.205	81.50	0.205	77.98	0.205	71.35
0.300	82.08	0.224	81.00	0.224	76.60	0.224	70.60
0.338	80.95	0.262	79.82	0.262	74.48	0.262	68.15
0.376	77.98	0.300	77.98	0.300	70.60	0.300	66.04
0.414	72.50	0.338	74.00	0.338	66.82	0.338	63.49
0.452	58.58	0.376	67.82	0.376	63.00	0.414	57.26
0.471	42.28	0.414	61.55	0.414	58.00	0.490	50.90
0.490	21.56	0.452	53.85	0.490	49.55	0.566	44.80
0.509	8.34	0.490	46.28	0.566	41.12	0.642	39.00
		0.528	38.40	0.642	31.32	0.718	32.78
		0.566	30.42	0.718	23.15	0.794	26.74
		0.604	23.15	0.794	16.78	0.870	21.18
		0.642	17.67	0.832	13.36	0.956	16.78
		0.780	11.58	0.870	10.62	1.032	11.58
		0.718	6.68	0.918	6.68	1.070	9.45
				0.937	3.27	1.108	6.68
						1.227	2.50

Table 5.4-2 (b)

Spread of the wall jet

x inches	$y_{\frac{1}{2}}$ inches	u_{max} ft/sec	x/y_c	$y_{\frac{1}{2}}/y_c$	u_{max}/u_c
0.00	0.450	83.22	0.00	0.95	1.000
1.97	0.536	81.82	4.16	1.13	0.983
3.94	0.584	79.00	8.32	1.23	0.950
5.91	0.591	74.65	12.48	1.25	0.897
7.88	0.636	71.58	16.64	1.34	0.860
9.85	0.690	57.85	20.80	1.45	0.695
11.82	0.750	53.85	24.96	1.58	0.646
13.79	0.807	50.00	29.12	1.71	0.600
15.76	0.866	45.80	33.28	1.83	0.550
19.70	0.985	40.10	41.60	2.08	0.481

Table 5.4-3 (a)

Velocity profile data

Rough surface (y_r = 0.37 mm) Slot opening = 3 mm. Slot Re=5.1×10^3

x = 0		x = 1.97"		x = 3.94"		x = 7.88"	
y inches	u ft/sec	y inches	u ft/sec	y inches	u ft/sec	y inches	u ft/sec
0.034	82.54	0.034	42.28	0.034	32.78	0.034	23.15
0.053	82.80	0.053	46.28	0.053	33.41	0.053	25.00
0.072	82.54	0.072	48.15	0.072	35.95	0.072	26.74
0.091	82.54	0.091	48.55	0.091	37.20	0.091	27.22
0.110	82.40	0.110	48.55	0.110	37.80	0.110	27.55
0.129	76.41	0.129	47.30	0.129	37.80	0.129	27.84
0.148	45.28	0.148	45.42	0.148	37.80	0.148	28.19
0.154	8.45	0.167	43.32	0.167	37.20	0.167	28.19
		0.186	41.44	0.186	36.60	0.186	28.19
		0.205	39.00	0.205	35.95	0.205	28.19
		0.224	35.95	0.224	35.38	0.224	28.19
		0.243	33.41	0.262	33.41	0.262	27.84
		0.262	30.42	0.300	30.42	0.300	27.55
		0.300	25.00	0.338	28.19	0.338	26.74
		0.338	18.90	0.376	25.88	0.376	25.88
		0.376	14.94	0.414	23.15	0.414	25.00
		0.414	11.58	0.452	21.18	0.490	23.15
		0.452	9.45	0.496	18.90	0.566	21.18
		0.490	6.68	0.528	16.78	0.642	18.90
				0.604	12.40	0.718	16.78
				0.642	9.45	0.832	13.36
				0.680	6.68	0.918	11.58
				0.718	4.27	0.994	9.45
						1.070	9.45
						1.146	6.68

Table 5.4-3 (b)

Spread of the wall jet

x inches	$y_{\frac{1}{2}}$ inches	u_{max} ft/sec	x/y_c	$y_{\frac{1}{2}}/y_c$	u_{max}/u_c
0.00	0.115	82.80	0.00	0.98	1.000
1.97	0.286	48.55	16.66	2.08	0.586
3.94	0.482	37.80	33.32	4.00	0.455
5.91	0.670	32.05	50.00	5.66	0.386
7.88	0.827	28.19	66.84	7.00	0.340
9.85	1.005	25.88	83.33	8.50	0.312
11.82	1.162	23.15	100.00	10.00	0.280
13.79	1.420	22.14	116.66	12.00	0.268
15.76	1.680	20.04	133.68	14.00	0.246
19.70	1.972	17.67	166.66	16.66	0.213
23.64	2.313	16.78	200.00	19.33	0.202

Table 5.4-4 (a)

Velocity profile data

Rough surface (y_r = 0.37 mm) Slot opening = 6 mm Slot Re=1.017×10^4

x = 0		x = 1.97"		x = 3.94"		x = 7.88"	
y inches	u ft/sec	y inches	u ft/sec	y inches	u ft/sec	y inches	u ft/sec
0.034	81.80	0.034	58.20	0.034	49.05	0.034	34.75
0.053	82.54	0.053	59.00	0.053	53.45	0.053	39.00
0.072	82.54	0.072	65.05	0.072	55.80	0.072	41.30
0.091	82.40	0.091	69.76	0.091	58.20	0.091	42.28
0.110	82.40	0.110	72.85	0.110	59.00	0.110	43.32
0.129	82.08	0.129	73.50	0.129	59.80	0.129	44.30
0.148	81.80	0.148	72.50	0.148	59.43	0.148	44.30
0.167	80.95	0.167	70.60	0.167	59.00	0.167	44.30
0.186	79.25	0.186	67.05	0.186	57.35	0.186	44.30
0.205	77.75	0.205	64.46	0.205	55.80	0.224	44.30
0.224	75.00	0.224	59.80	0.224	55.05	0.262	43.32
0.243	45.42	0.243	56.60	0.243	52.20	0.300	42.28
0.262	8.65	0.262	51.35	0.262	50.50	0.338	41.12
		0.281	48.15	0.300	46.28	0.376	39.55
		0.300	44.30	0.338	42.28	0.414	37.80
		0.338	36.60	0.376	37.20	0.490	34.08
		0.376	29.85	0.414	33.41	0.566	29.85
		0.414	23.15	0.452	29.10	0.642	26.74
		0.490	11.58	0.490	25.00	0.718	22.14
		0.528	6.68	0.528	21.18	0.794	18.90
				0.604	14.94	0.870	16.78
				0.680	9.45	0.956	13.36
				0.718	6.68	1.032	10.51
						1.070	9.45
						1.108	7.54
						1.146	6.68

Table 5.4-4 (b)

Spread of the wall jet

x inches	$y_{\frac{1}{2}}$ inches	u_{max} ft/sec	x/y_c	$y_{\frac{1}{2}}/y_c$	u_{max}/u_c
0.00	0.245	82.54	0.00	0.91	1.000
1.97	0.350	73.50	8.33	1.48	0.890
3.94	0.462	59.80	16.66	1.95	0.725
5.91	0.610	51.35	25.00	2.58	0.621
7.88	0.744	44.80	33.32	3.14	0.542
9.85	0.896	38.40	41.65	3.75	0.465
11.82	1.062	33.41	50.00	4.36	0.404
13.79	1.181	29.85	58.31	5.00	0.362
15.76	1.370	28.19	66.64	5.64	0.343
19.70	1.670	24.08	83.33	6.91	0.292
23.64	1.950	19.12	100.00	8.25	0.232

Table 5.4-5 (a)

Velocity profile data

Rough surface (y_r=0.31mm) Slot opening=3mm. Slot Re=5.16×10^3

x = 0		x = 1.97"		x = 3.94"		x = 7.88"	
y inches	u ft/sec	y inches	u ft/sec	y inches	u ft/sec	y inches	u ft/sec
0.034	83.50	0.034	51.60	0.034	39.00	0.034	28.19
0.053	83.70	0.053	53.45	0.053	41.64	0.053	29.10
0.072	84.00	0.072	59.00	0.072	43.78	0.072	29.85
0.091	83.50	0.091	59.80	0.091	44.30	0.091	29.85
0.110	82.08	0.110	59.00	0.110	44.80	0.110	30.42
0.129	79.90	0.129	57.05	0.129	44.80	0.129	30.42
0.148	12.45	0.148	54.25	0.148	43.78	0.148	30.42
		0.167	51.35	0.167	42.78	0.167	30.42
		0.186	48.15	0.186	41.64	0.186	29.85
		0.205	44.30	0.205	40.10	0.224	29.85
		0.224	41.44	0.224	38.40	0.262	29.10
		0.243	37.80	0.243	37.20	0.300	28.19
		0.262	34.75	0.262	35.95	0.338	28.19
		0.300	28.19	0.300	32.78	0.376	27.55
		0.338	22.14	0.338	29.85	0.414	26.74
		0.376	16.78	0.376	26.74	0.490	25.00
		0.414	11.58	0.414	23.15	0.566	22.14
		0.452	9.50	0.452	21.18	0.642	18.90
		0.490	6.68	0.528	16.78	0.718	16.78
				0.604	12.46	0.794	14.94
				0.680	9.45	0.918	11.58
				0.756	6.68	0.994	9.45
						1.108	6.68

Table 5.4-5 (b)

Spread of the wall jet

x inches	$y_{\frac{1}{2}}$ inches	u_{max} ft/sec	x/y_c	$y_{\frac{1}{2}}/y_c$	u_{max}/u_c
0.00	0.135	84.00	0.00	0.932	1.000
1.97	0.300	59.80	16.66	2.54	0.712
3.94	0.448	44.80	33.32	3.79	0.534
5.91	0.685	34.75	50.00	5.79	0.413
7.88	0.841	30.42	66.84	7.12	0.362
9.85	1.060	26.74	83.33	8.96	0.318
11.82	1.256	24.08	100.00	10.62	0.286
13.79	1.413	22.14	116.66	11.96	0.265
15.76	1.530	21.18	133.68	12.96	0.252
19.70	1.810	18.90	166.66	15.27	0.225
23.64	2.160	16.78	200.00	18.29	0.199

Table 5.4-6 (a)

Velocity profile data

Rough surface (y_r=0.31mm). Slot opening=6mm. Slot Re=1.028×10^4

x = 0		x = 1.97"		x = 3.94"		x = 7.88"	
y inches	u ft/sec	y inches	u ft/sec	y inches	u ft/sec	y inches	u ft/sec
0.034	82.80	0.034	69.05	0.034	59.80	0.034	42.78
0.053	83.22	0.053	76.60	0.053	64.80	0.053	44.80
0.072	83.50	0.072	79.62	0.072	66.82	0.072	46.77
0.091	83.50	0.091	80.74	0.091	68.50	0.091	48.15
0.110	83.22	0.110	79.62	0.110	68.15	0.110	48.55
0.129	82.80	0.129	78.20	0.129	67.45	0.129	49.05
0.148	82.40	0.148	75.68	0.148	66.04	0.148	49.05
0.167	80.74	0.167	73.20	0.167	64.80	0.167	49.55
0.186	79.62	0.186	70.00	0.186	62.65	0.186	49.55
0.205	77.75	0.205	66.82	0.205	60.59	0.224	48.55
0.224	75.40	0.224	62.45	0.224	58.20	0.262	47.30
0.243	35.38	0.262	55.50	0.262	53.85	0.300	45.42
0.262	9.45	0.300	48.15	0.300	49.05	0.338	43.32
		0.338	41.44	0.338	44.80	0.376	41.64
		0.376	32.78	0.376	40.10	0.414	40.10
		0.414	25.88	0.414	34.75	0.490	35.95
		0.452	20.04	0.452	29.85	0.566	31.32
		0.490	13.36	0.490	25.88	0.642	26.74
		0.528	9.45	0.528	21.18	0.718	23.15
				0.566	17.67	0.794	18.90
				0.604	13.36	0.870	14.94
				0.642	11.58	0.956	13.36
				0.680	9.45	1.032	9.45
				0.718	6.68	1.108	6.68

Table 5.4-6 (b)

Spread of the wall jet

x inches	$y_{\frac{1}{2}}$ inches	u_{max} ft/sec	x/y_c	$y_{\frac{1}{2}}/y_c$	u_{max}/u_c
0.00	0.232	83.50	0.00	0.93	1.000
1.97	0.350	80.74	8.33	1.48	0.965
3.94	0.448	68.50	16.66	1.89	0.820
5.91	0.625	57.26	25.00	2.64	0.685
7.88	0.725	49.55	33.82	3.06	0.594
9.85	0.861	43.78	41.65	3.64	0.524
11.82	1.040	39.55	50.00	4.31	0.473
13.79	1.178	36.60	58.31	4.98	0.438
15.76	1.373	32.78	66.64	5.81	0.392
19.70	1.610	29.85	83.33	6.81	0.358
23.64	1.924	25.88	100.00	8.14	0.310

Table 5.4-7 (a)

Velocity profile data

Rough surface (y_r=0.13mm) Slot opening=2mm Slot Re=3.43×10^3

x = 0		x = 3.94"		x = 7.88"	
y inches	u ft/sec	y inches	u ft/sec	y inches	u ft/sec
0.034	83.50	0.034	25.88	0.034	17.67
0.043	83.70	0.053	26.74	0.053	17.67
0.053	83.70	0.072	27.55	0.072	18.24
0.062	80.70	0.091	28.19	0.091	18.90
0.072	83.22	0.110	29.10	0.110	20.04
0.081	68.75	0.129	28.19	0.129	20.66
0.091	58.20	0.148	27.55	0.148	20.66
0.100	38.42	0.167	26.74	0.167	20.04
0.110	9.46	0.186	26.74	0.186	20.04
		0.224	25.88	0.224	20.04
		0.262	24.08	0.262	18.90
		0.338	21.18	0.338	18.90
		0.414	17.67	0.414	17.67
		0.490	16.78	0.490	16.78
		0.566	13.36	0.604	14.94
		0.642	9.45	0.718	13.36
		0.718	6.68	0.832	11.58
				0.956	9.45
				1.070	6.68

Table 5.4-2 (h)

Spread of the wall jet

x inches	$y_{\frac{1}{2}}$ inches	u_{max} ft/sec	x/y_c	$y_{\frac{1}{2}}/y_c$	u_{max}/u_o
0.00	0.105	83.70	00.00	1.34	1.000
1.97	0.315	39.00	25.00	4.00	0.465
3.94	0.547	29.10	50.00	6.95	0.348
5.91	0.710	23.15	75.00	9.00	0.286
7.88	0.920	20.66	100.00	11.69	0.246
9.85	1.104	17.67	125.00	14.00	0.211
11.82	1.340	16.78	150.00	17.00	0.200
13.79	1.500	14.94	175.00	19.00	0.178
15.76	1.675	13.36	200.00	21.25	0.160

Table 5.4-8 (a)

Velocity profile data

Rough surface (y_r=.13mm) Slot opening=8mm Slot Re=1.355×10^4

x = 0		x = 3.94"		x = 7.88"	
y inches	u ft/sec	y inches	u ft/sec	y inches	u ft/sec
0.034	81.50	0.034	55.05	0.034	43.32
0.053	81.80	0.053	57.26	0.053	45.42
0.072	82.80	0.072	60.50	0.072	47.30
0.091	83.22	0.091	62.65	0.091	48.15
0.110	82.80	0.110	63.49	0.110	49.05
0.129	82.80	0.129	63.68	0.129	50.00
0.148	82.40	0.148	64.05	0.148	50.00
0.167	82.08	0.167	63.49	0.167	49.55
0.186	81.80	0.186	61.95	0.186	49.05
0.205	80.74	0.224	59.00	0.224	48.15
0.224	79.82	0.262	55.05	0.262	46.77
0.262	76.41	0.338	48.15	0.300	46.28
0.300	30.42	0.414	39.55	0.338	44.30
0.338	9.45	0.490	31.32	0.414	41.12
		0.566	22.14	0.490	36.60
		0.642	16.78	0.604	31.32
		0.718	9.45	0.718	25.00
		0.832	6.68	0.794	18.90
				0.956	14.94
				1.070	9.45
				1.146	6.68

Table 5.4-3 (b)

Spread of the wall jet

x inches	$y_{\frac{1}{2}}$ inches	u_{max} ft/sec	x/y_c	$y_{\frac{1}{2}}/y_c$	u_{max}/u_c
0.00	0.242	83.22	0.00	0.76	1.000
1.97	0.354	74.00	6.25	1.12	0.887
3.94	0.507	64.05	12.50	1.61	0.770
5.91	0.670	55.50	18.75	2.12	0.667
7.88	0.745	50.00	25.00	2.36	0.600
9.85	0.905	44.30	31.25	2.87	0.532
11.82	1.043	39.00	37.50	3.31	0.468
13.79	1.180	36.60	43.75	3.75	0.439
15.76	1.300	33.41	50.00	4.12	0.401

CHAPTER - 6

RESULTS OF THE EXPERIMENTAL INVESTIGATION

6.1 Introduction

In the present Chapter, we shall present the results of our experimental investigation and compare the same with the theoretical predictions. We shall also compare the results of the radial wall-jet by Jayatillaka[8] with our predictions.

6.2 Plane wall-jet

A set of measured velocity profiles on the smooth surface is shown in Figure 6.2-1, and a set on the rough surface (y_r = 0.37 mm) in Figure 6.2-2. They both have the same general appearance. Typical slot velocity profiles are shown in Figure 6.2-3.

6.2-1 Growth of the jet and decay of the maximum velocity

A set of experimental results on both smooth and rough surfaces for different slot heights are shown in Figures 6.2-4 to 6.2-11. In all these figures the full line represents the theoretical prediction. The explanation of the various notations are:

- x - distance from the slot
- Y_c - slot height
- $Y_{\frac{1}{2}}$ - value of y where the velocity is half the maximum
- u_c - maximum velocity at the slot

The agreement between the experimental results and the theoretical predictions are seen to be satisfactory in all the cases.

6.2-2 Velocity profiles

Velocity profiles on a non-dimensional basis for various cases with the corresponding theoretically predicted profiles are shown in Figures 6.2-12 to 6.2-15 . Again, we observe a good agreement between the theory and the experiment.

6.3 Radial wall-jet

The theoretical predictions in the previous cases were made with the following values for the mixing-length constants: $k = 0.435$ and $\lambda = 0.09$. These values have been recommended by Patankar[12] after comparing the theoretical predictions with certain well-known experimental results. However, for the case of a radial wall jet, it is recommended that the constants should be $\sqrt{2}$ times larger than those for the plane one. The reason given is that the effective viscosity in a radial wall jet is twice as large as that in a plane wall jet. We have used these modified values of the constants for the purpose of comparison with the radial wall jet results of Jayatillaka[8].

6.3-1 Growth of the jet and decay of the maximum velocity

Figures 6.3-1 to 6.3-4[2] show the experimental results of Jayatillaka[8] and our theoretical predictions for various cases. We see that the agreement between the two is satisfactory.

6.3-2 Velocity profiles

The experimental velocity profiles with the corresponding ones by our predictions are shown in Figures 6.3-3 and 6.3-4. Again, we find that there exists good agreement between the experimental results and our predictions.

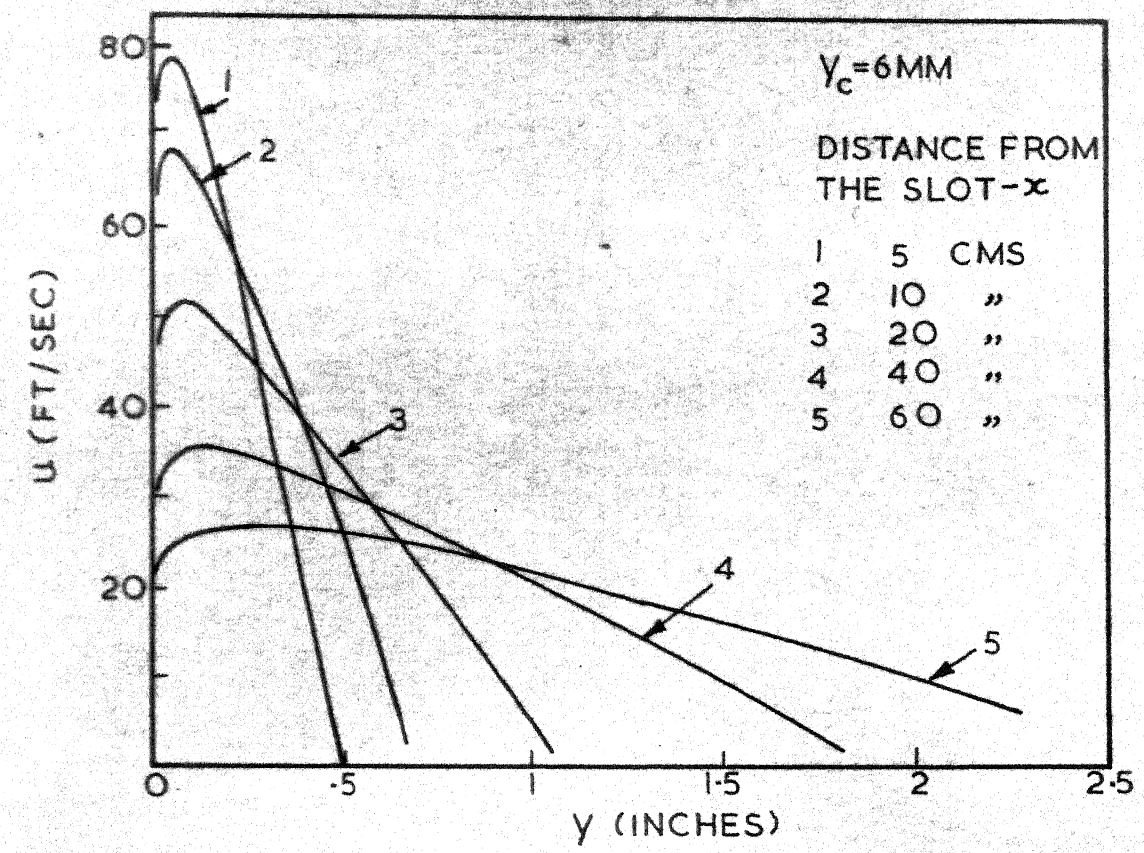

FIG. 6·2-1 MEASURED VELOCITY PROFILES (PLANE WALL JET ON SMOOTH SURFACE)

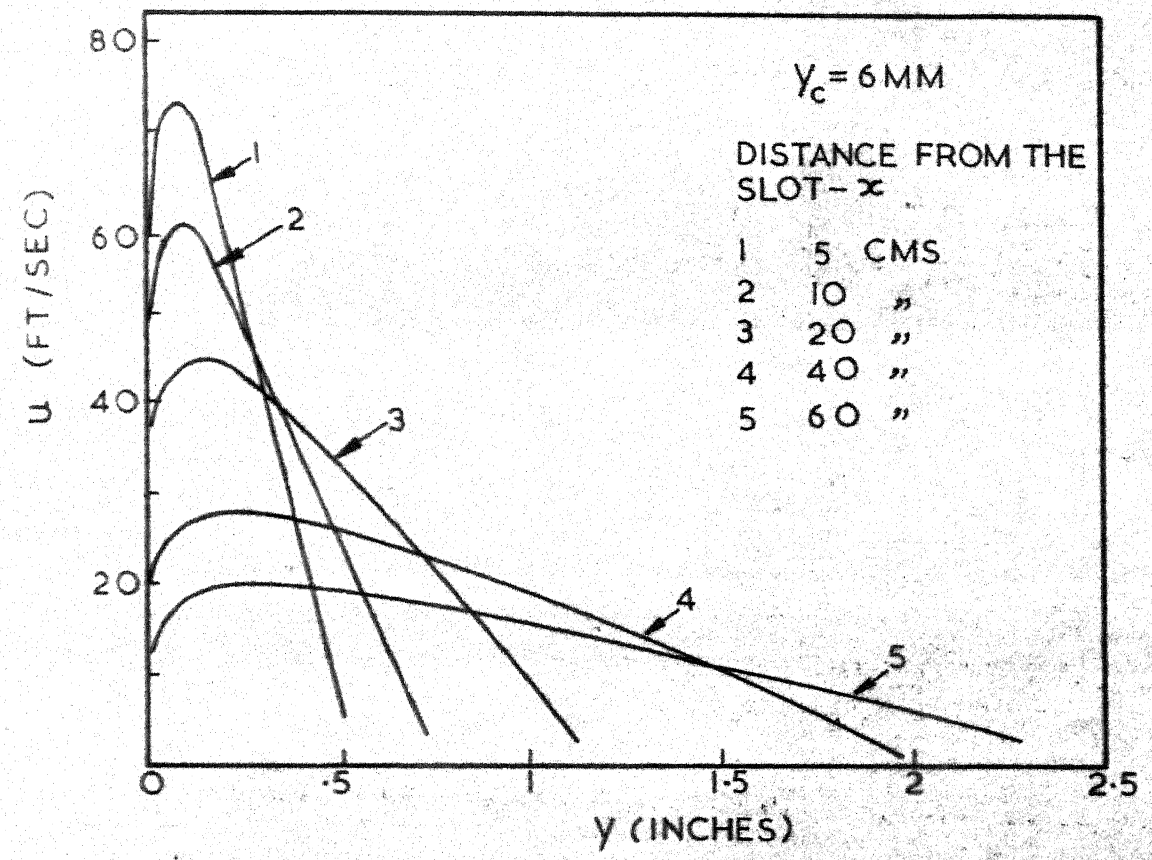

FIG. 6·2-2 MEASURED VELOCITY PROFILES(PLANE WALL JET ON ROUGH SURFACE, y_r=0·37 MM)

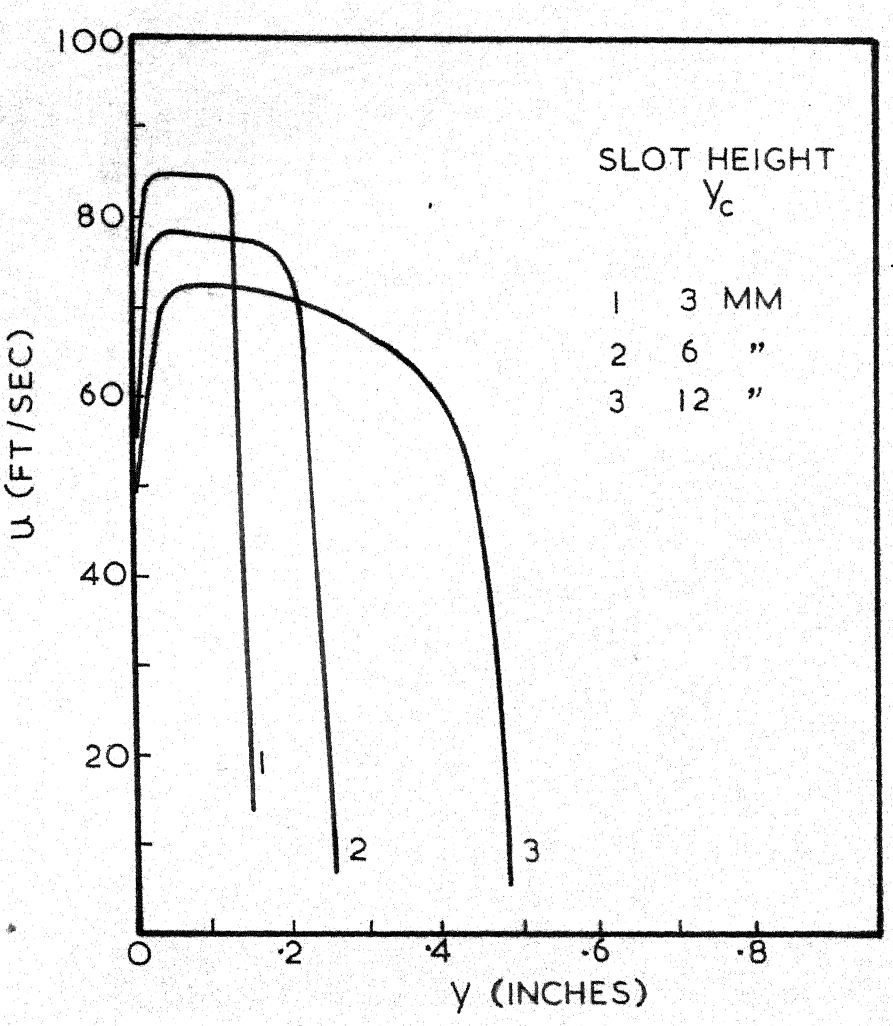

FIG. 6·2-3 VELOCITY PROFILES AT SLOT

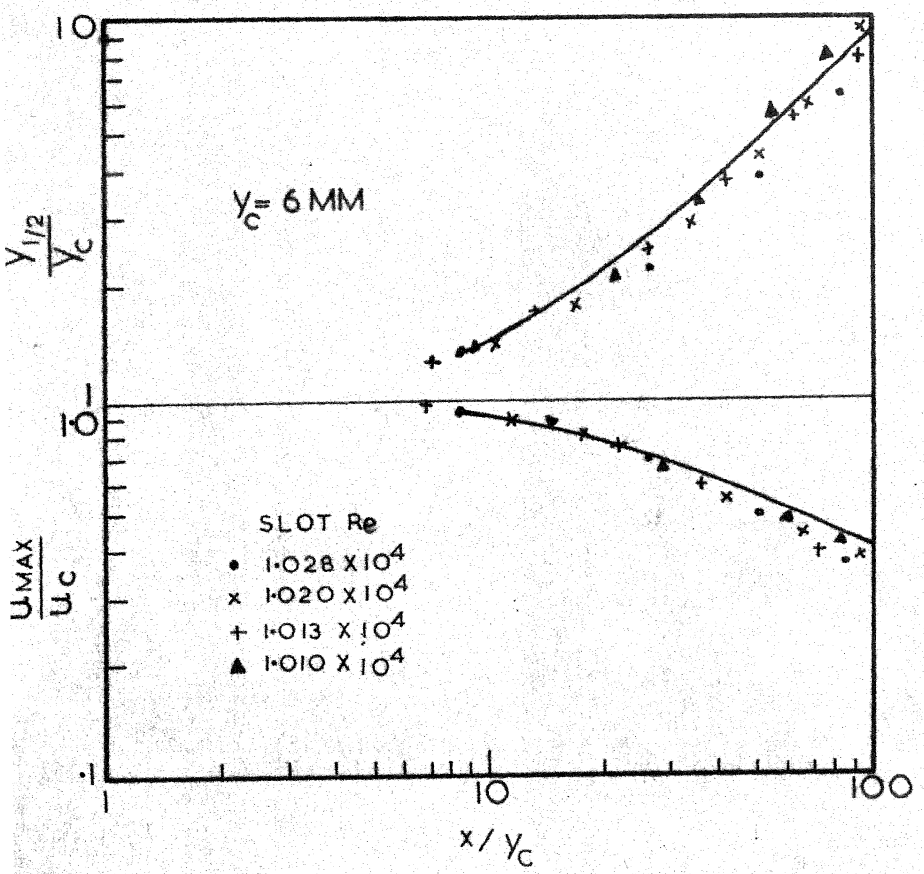

FIG. 6·2-4 WALL JET GROWTH AND VELOCITY DECAY (SMOOTH SURFACE)

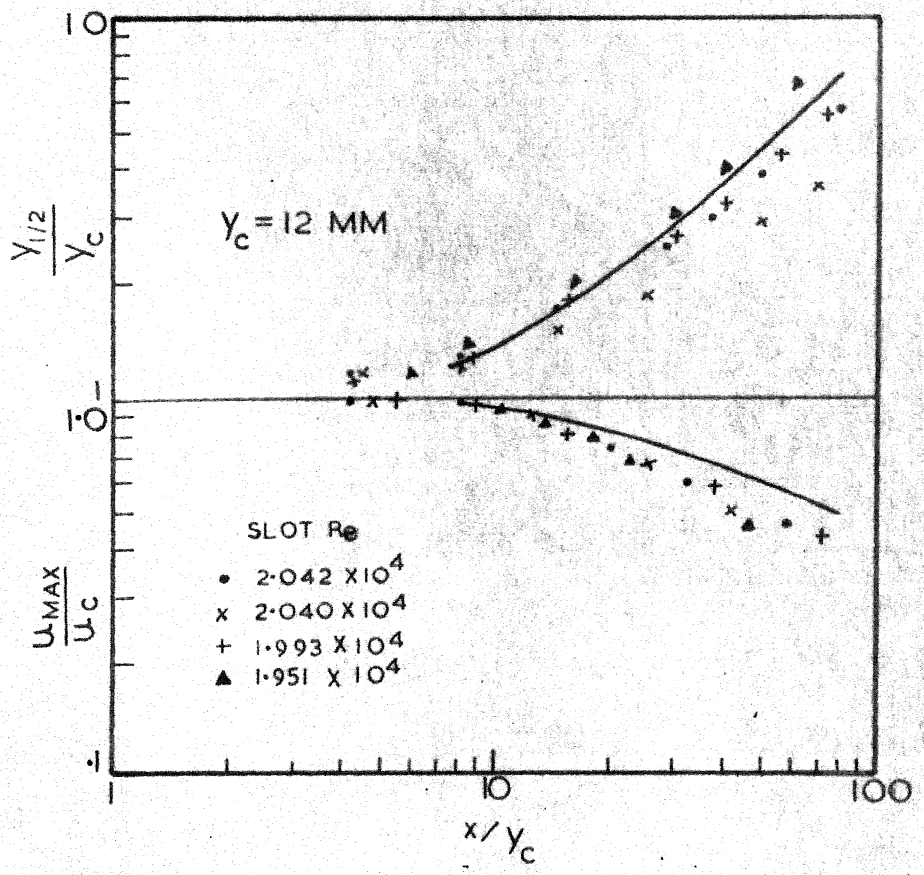

FIG. 6·2-5 WALL JET GROWTH AND VELOCITY DECAY (SMOOTH SURFACE)

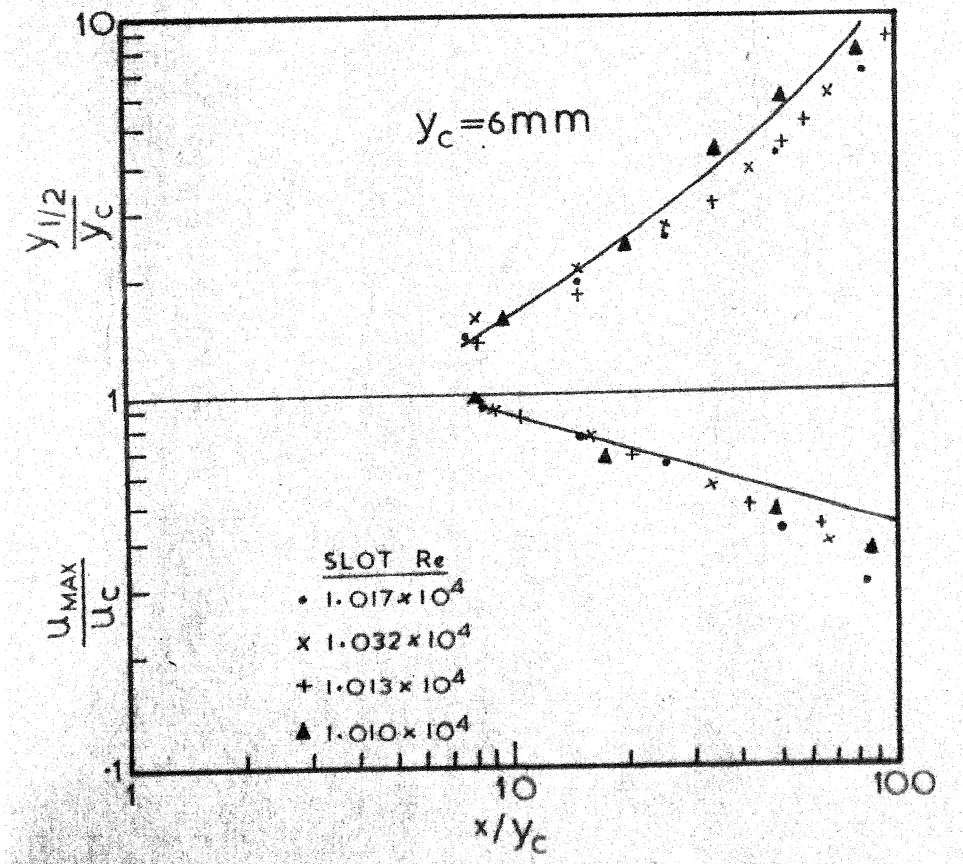

FIG.6·2-6 WALL JET GROWTH AND VELOCITY DECAY, ROUGH SURFCE (y_r = 0·37mm)

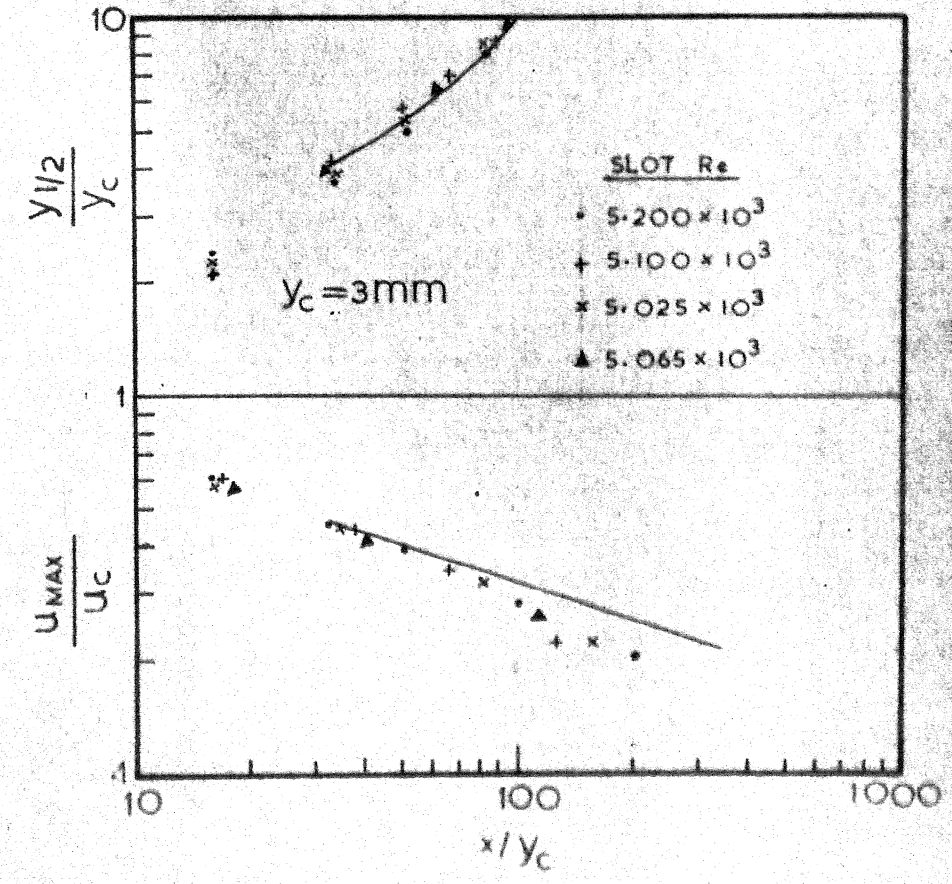

FIG.6·2-7 WALL JET GROWTH AND VELOCITY DECAY, ROUGH SURFACE (y_r = 0·37mm)

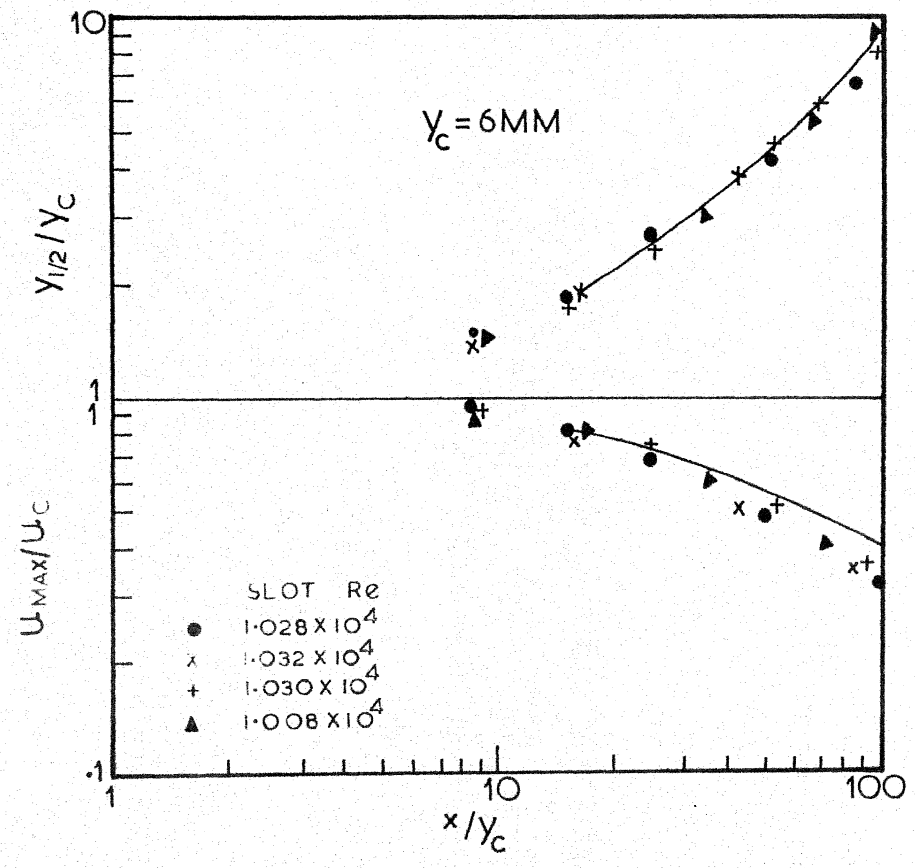

FIG. 6·2-8 WALL JET GROWTH AND VELOCITY DECAY, ROUGH SURFACE (y_r=0·31 mm)

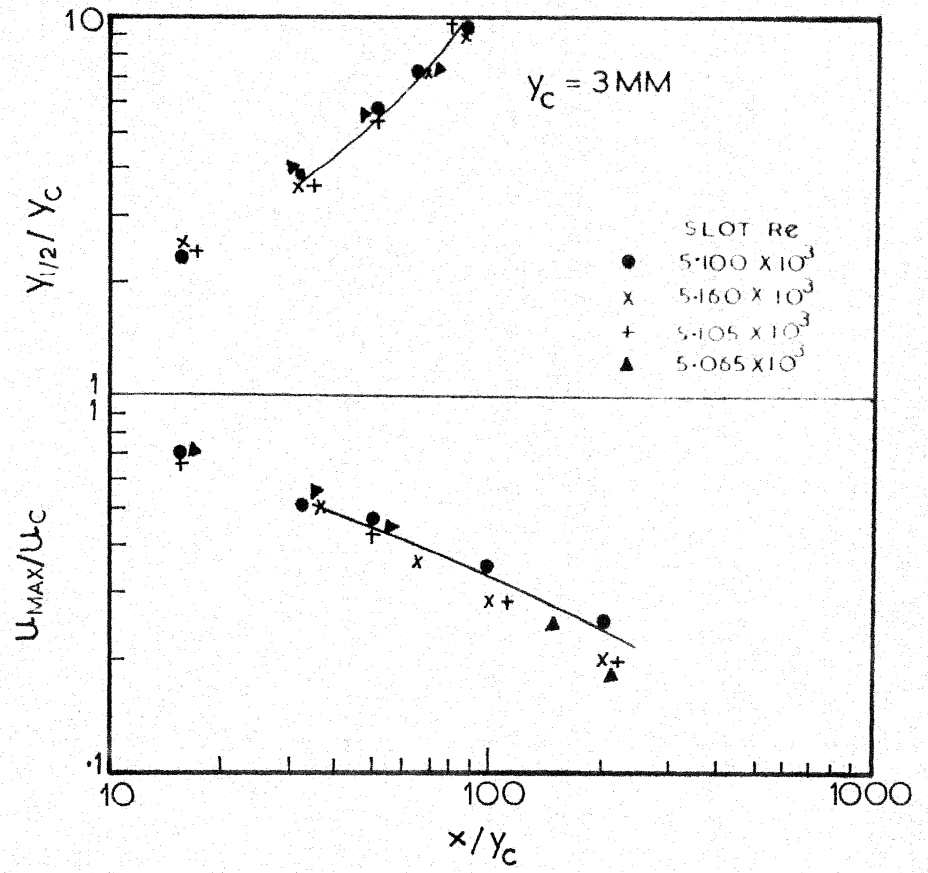

FIG. 6·2-9 WALL JET GROWTH AND VELOCITY DECAY, ROUGH SURFACE (y_r = 0·31 mm)

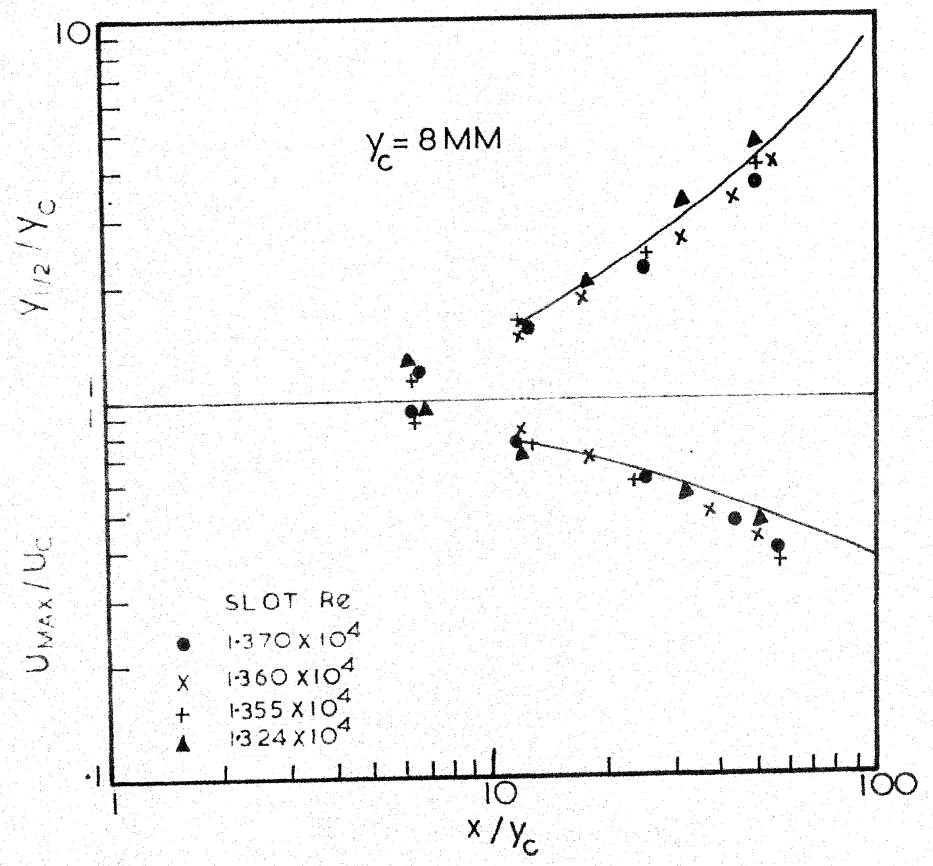

FIG. 6·2-10 WALL JET GROWTH AND VELOCITY-DECAY, ROUGH SURFACE(y_r=0·13mm)

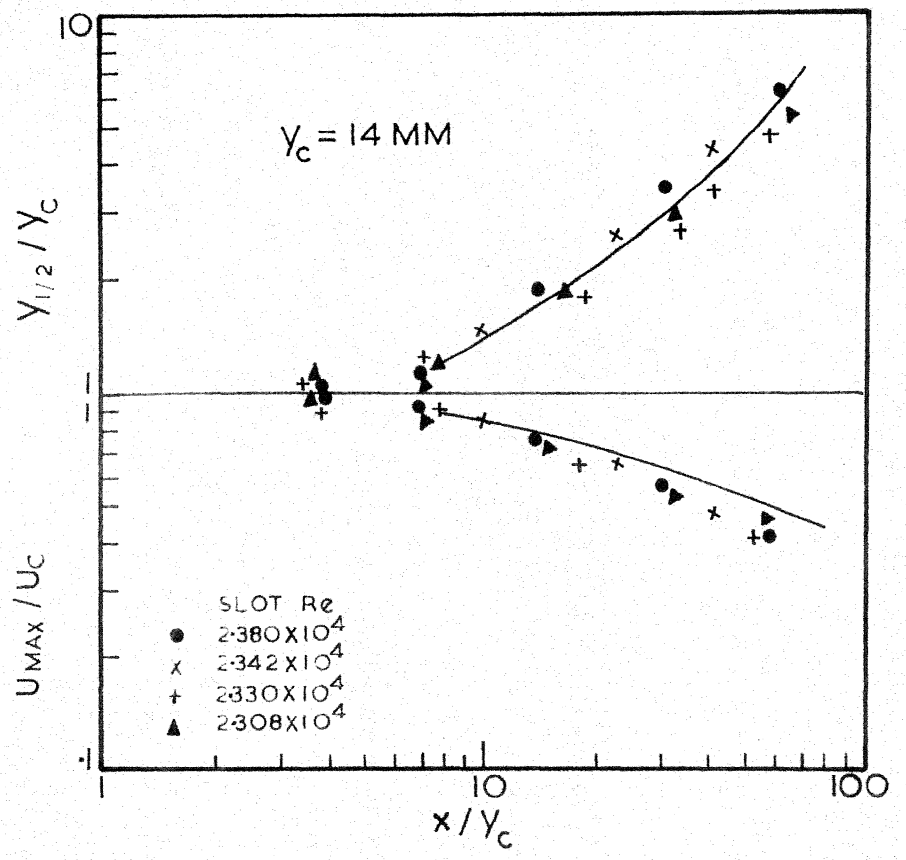

FIG. 6·2-11 WALL JET GROWTH AND VELOCITY-DECAY, ROUGH SURFACE(y_r=0·13mm)

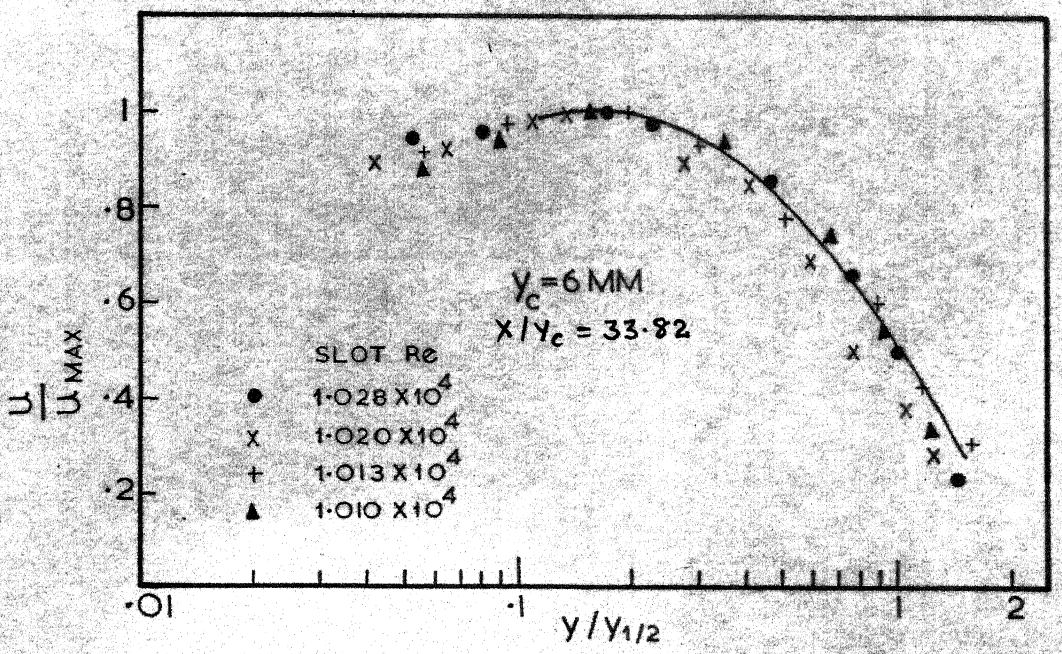

FIG. 6·2-12 VELOCIY PROFILES (SMOOTH SURFACE)

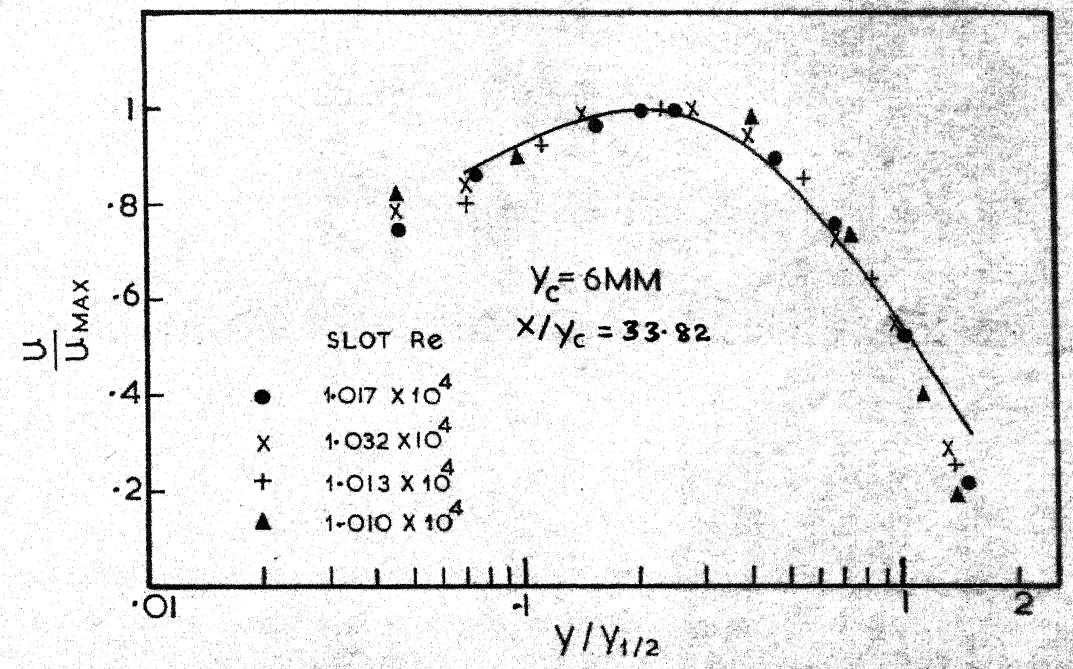

FIG. 6·2-13 VELOCITY PROFILES (ROUGH SURFACE : y_r=0·37MM)

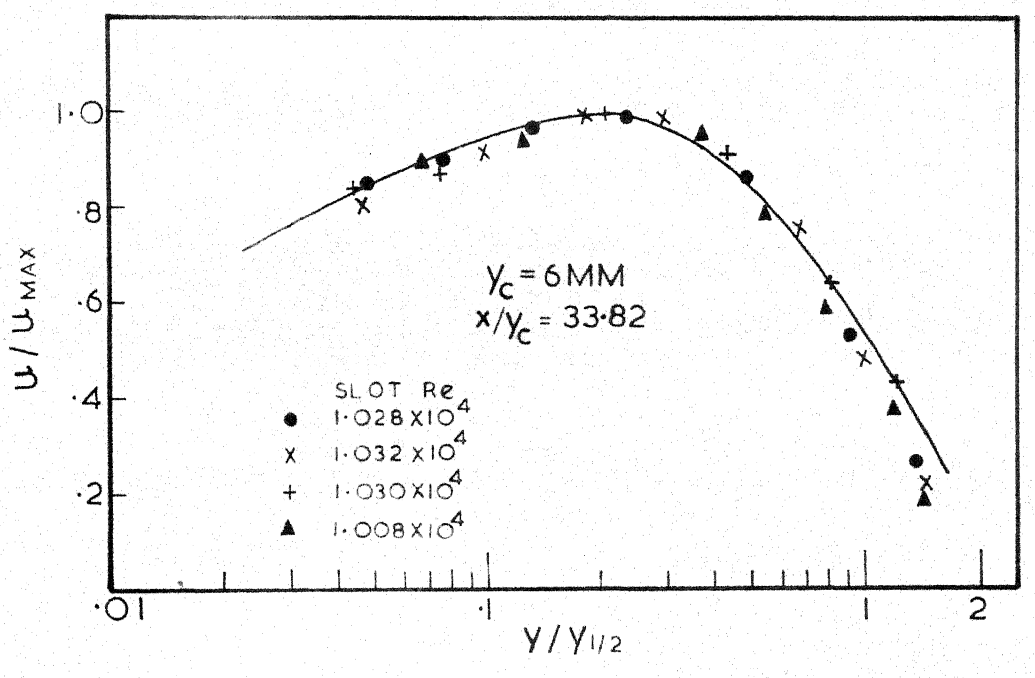

FIG. 6·2-14 VELOCITY PROFILES (ROUGH SURFACE: y_r = 0·31 MM)

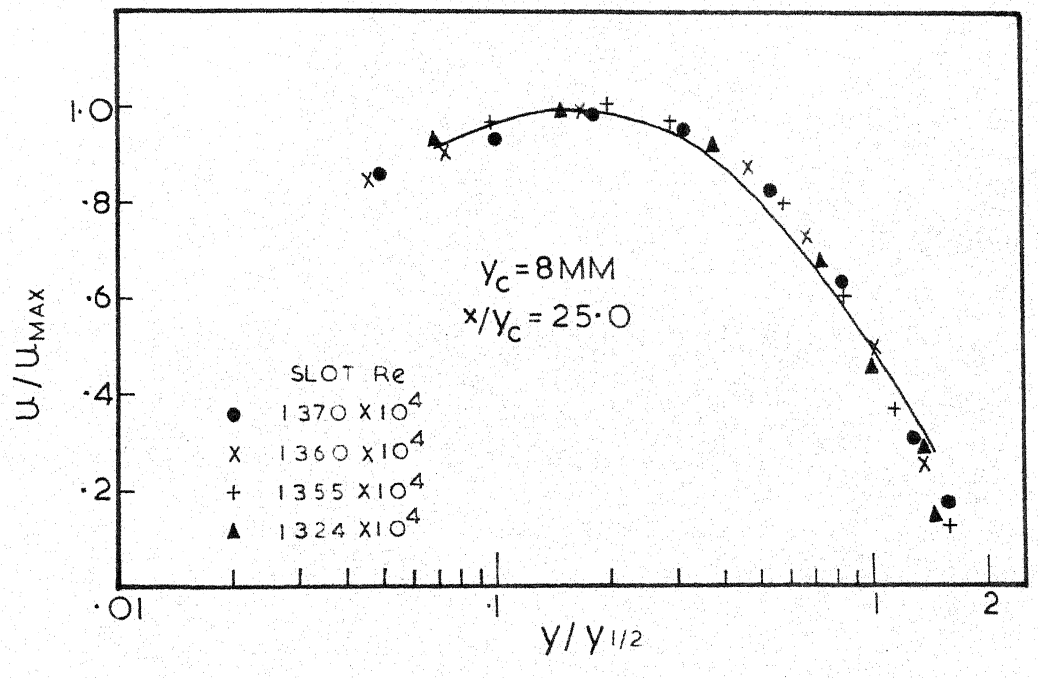

FIG. 6·2-15 VELOCITY PPOFILES (ROUGH SURFACE: y_r = 0·13 MM)

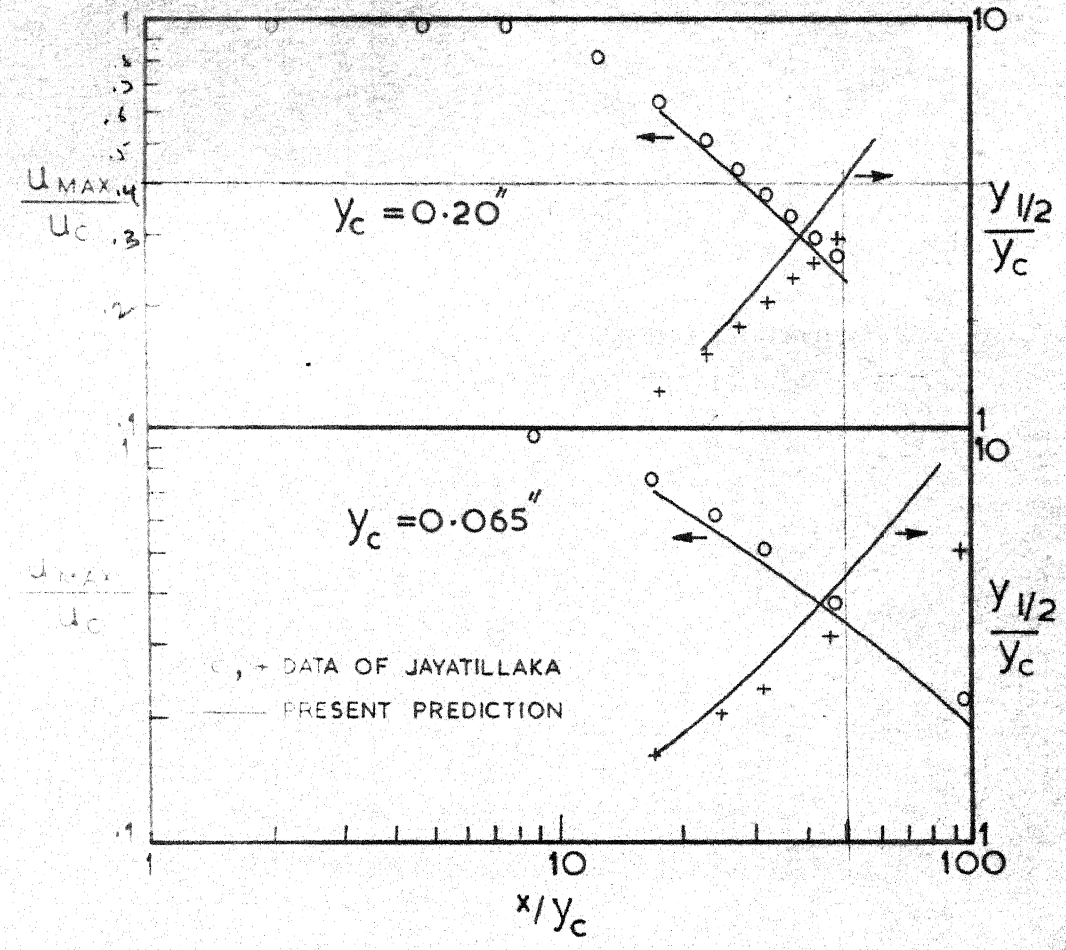

FIG. 6.3-1 WALL JET GROWTH AND VELOCITY DECAY, SMOOTH SURFACE.

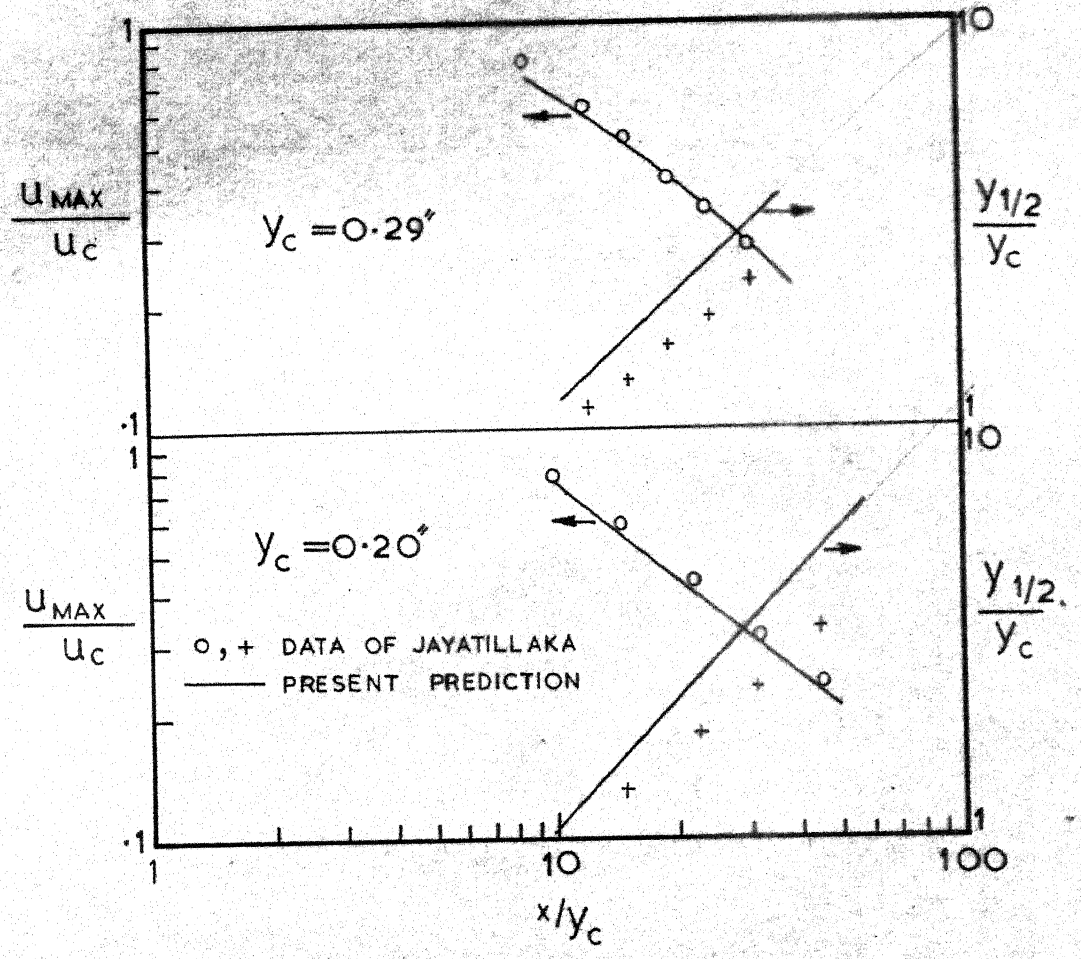

FIG.6.3-2 WALL JET GROWTH AND VELOCITY DECAY, EMERY SURFACE. ($y_r = 0.0082''$)

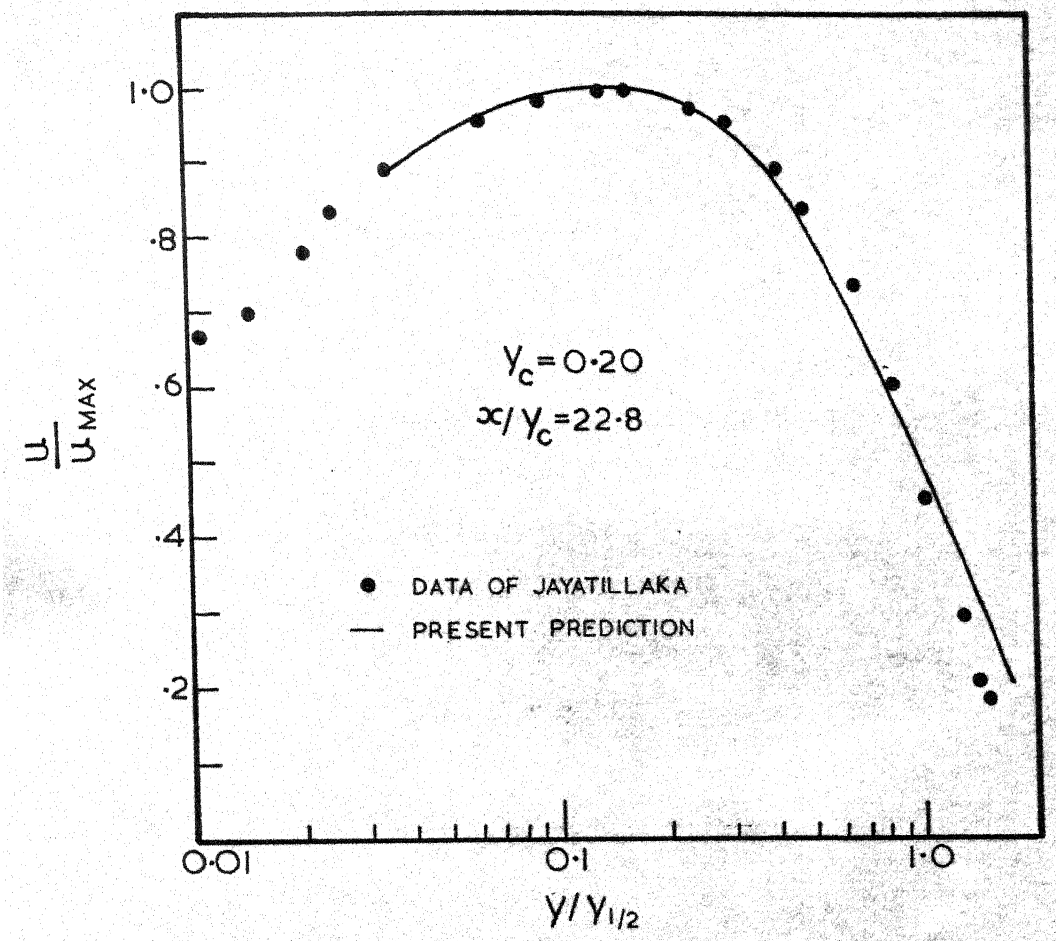

FIG. 6-3-3 RADIAL WALL JET VELOCITY PROFILE (SMOOTH SURFACE)

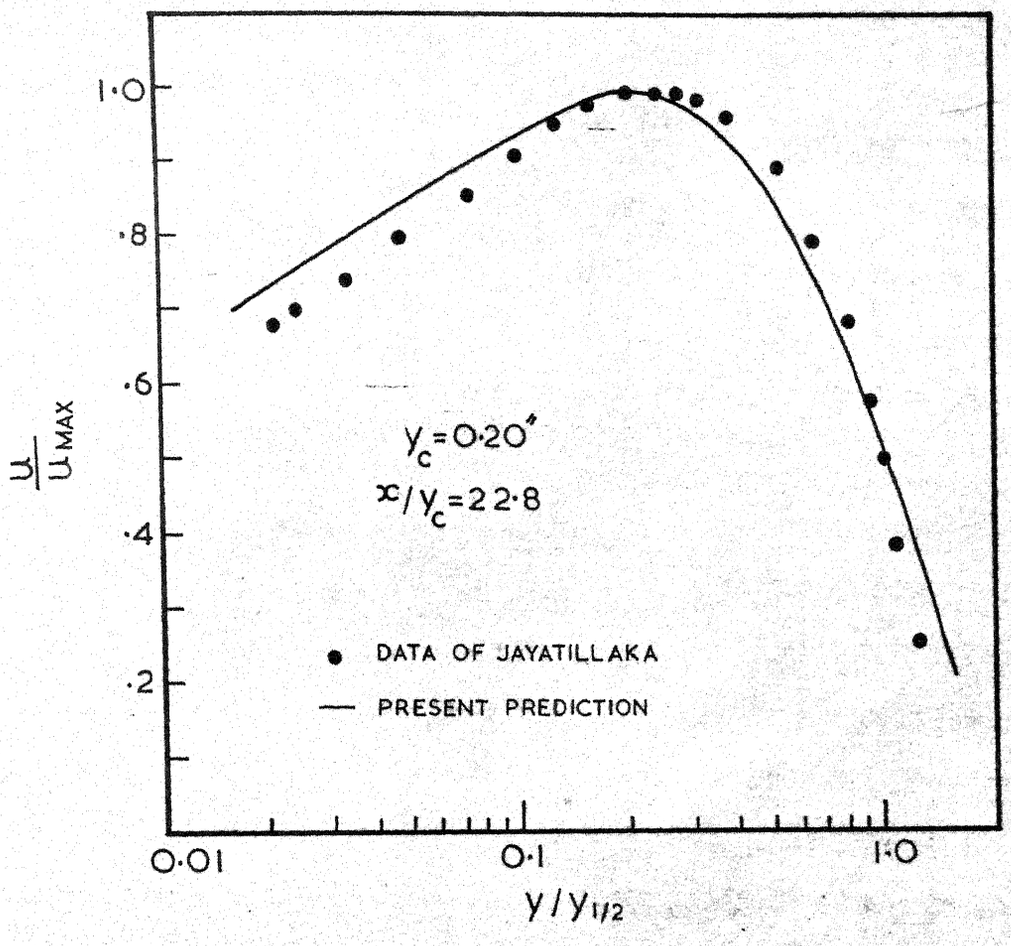

FIG. 6·3-4 RADIAL WALL JET VELOCITY PROFILE (EMERY SURFACE)

CHAPTER - 7

CONCLUDING REMARKS

It has been shown how the problem of the turbulent boundary layer flow with surface roughness can be solved by the finite-difference method. The modification begins with a logarithmic law velocity distribution for the wall region and incorporates a roughness parameter, the expressions for which are obtained from the pipe-flow measurements.

Various types of roughness have been classified and the roughness effects for two types have been predicted. For a flow, with the velocity being the same, the skin-friction and the Stanton number and hence the heat transfer rate can be increased by increasing the height of the roughness elements on the surface. The maximum amount of roughness admissible for a given situation can be determined. On the other hand, in cases where the roughness of the surface is not desirable, the maximum amount of roughness which can still maintain hydrodynamic smoothness of the surface can be calculated. This would help to determine the amount of labour worth spending in manufacturing a given surface.

Some experiments on a plane wall jet over a rough surface are also reported and it has been found that there is satisfactory agreement between the theory and the experiment.

The problem can be extended in various directions.

Predictions can be made for all the available types of roughness and the results compared. The effective type for a given situation can be determined. On the experimental side, temperature measurements in the plane wall jet case can be made and the results compared with the theory. The problem can be extended to cases with pressure gradients. Perry and Joubert[13] have carried out experiments on rough wall boundary layers in adverse pressure gradients and these results can be compared. The problem can also be extended to cases with varying fluid properties and mass transfer through the wall.

REFERENCES

1 AMBROSE, H.H. (1956) " The effect of surface roughness on velocity distribution and boundary resistance ". University of Tennessee, Department of Civil Engineering, contract N/r 811 (03) , Office of Naval Research, Department of the Navy.

2 BETTERMANN, D. " Contribution l'etude de la couche limite turbulente le long de plaques rugueuses ". Centre National de la Recherche Scientifique, Faculte des Sciences de Pavis, Laboratoire Aerothermique, Rapport No. 65-6.

3 CHI, S.W. and SPALDING, D.B. (1964) " The drag of a compressible turbulent boundary layer on a smooth flat plate with and without heat transfer ". Journal of Fluid Mechanics, 18 , 117-143.

4 COLEBROOK, C.F. (1938/39) " Turbulent flow in pipes with particular reference to the transition region between the smooth and rough pipe laws ". Journal of the Institution of Civil Engineers, Vol. 11, 133-156.

5 COPE, W.F. (1941) " The friction and heat transmission coefficients of rough pipes ". Proc. Inst. Mechanical Engineers, Vol. 145, 99-105.

6 DIPPREY, D.F. and SABERSKY, R.H. (1963) " Heat and momentum transfer in smooth and rough tubes at various Prandtl numbers ". Int.J. Heat Mass Transfer, Vol. 6, 5 , 329-353.

7 DOENECKE, J. (1963) " Contribution a l'etude de la convection forcee turbulente le long de plaques rugueuses ". These, Faculte des Sciences, Paris.

8 JAYATILLAKA, C.L.V. (1966) " The influence of Prandtl number and surface roughness on the laminar sublayer to momentum and heat transfer ". Ph. D. Thesis, Imperial College of Science and Technology, London.

9 KOLAR, V. (1961) " Heat and momentum transfer in a turbulent medium ". Collection Czechoslov. Chem. Commun., Vol. 26, 335-345.

10 MALHERBE, J.M. (1963) " Influence des rugosite de paroi sur les coefficients d'echange thermique et de perte de charge ". Centre d'Etudes Nucleaires de Saclay, Rapport C.E.A, No. 2283.

11 NIKURADSE, J. (1933) " Stromungsgesetze in rauhen Rohren ". VDI Forschungsheft, 361.

12 PATANKAR, S.V. (1967) " Heat and mass transfer in turbulent boundary layers ". Ph.D. Thesis, Faculty of Engineering, University of London.

13 PERRY, A.E. and JOUBERT, P.N. (1963) " Rough wall boundary layers on adverse pressure gradients ". J. Fluid Mechanics, Vol. 17, 193-211.

14 SAMS, E.W. (1952) " Experimental investigation of average heat transfer and friction coefficients for air flowing in circular tubes having square thread type roughness ". NACA RM E52D17.

15 SCHLICHTING, H. (1960) Boundary Layer Theory, 4th Ed., McGraw Hill, New York.

16 STAMFORD, S. (1958) " The effect of roughness on the heat transfer from the pipe to a moving fluid ". Ph.D. Thesis, University of London.